**ABSTRACT**

SATCHER, MELINDA RENEE. De-bottlenecking the Electrospinning Process Using Superparamagnetic Particles. (Dr. Juan Hinestroza and Dr. Saad Khan.).

Nanocomposite polyethylene oxide (PEO) fibers containing magnetic domains were produced using parallel plate electrospinning. The fibers were spun from solutions dosed with nanoparticles of magnetite ($Fe_3O_4$) in 2wt% PEO in water. Solution parameters like viscosity, conductivity, and surface tension were measured and correlated to final fiber diameter. Increased amounts of magnetic nanoparticles produced higher conductivity, higher viscosity, and lower surface tension solutions.

Transmission electron microscopy and energy dispersive spectroscopy were used to analyze the diameters of the nanofibers as well as the distribution of the magnetic nanoparticles inside the PEO matrix. A SQUID magnetometer was applied to determine the AC and DC magnetic susceptibility of the fibers. The resultant nanofibers had diameters as low as 100 nm and exhibited unique AC susceptibility patterns and magnetic responses making them excellent for anti-counterfeiting applications.

.

# DE-BOTTLENECKING THE ELECTROSPINNING PROCESS USING SUPERPARAMAGNETIC PARTICLES

by

Melinda Renee Satcher

A thesis submitted to the Graduate Faculty of

North Carolina State University

In partial fulfillment of the

Requirements for the degree of

Master of Science

In

Textile Engineering

Raleigh, NC

2006

Approved by:

Dr. Juan Hinestroza
Co-Chair of Advisory Committee

Dr. Saad Khan
Co-Chair of Advisory Committee

Dr. William Oxenham
Committee Member

Dr. Lei Qian
Committee Member

**DEDICATION**

This work is dedicated to my father, the late Larry Satcher. My father passed away in November of 2005 while I was working on this research. His love and encouragement are the only reasons I finished this thesis.

Dad, I know my thesis completion meant more to you than it did to anyone else.

## BIOGRAPHY

Melinda Renee Satcher was born in November of 1979 in Macon, GA to Larry and Barbara Satcher. Melinda is the youngest of three children; she has an older brother and sister. After graduating from Southwest High School, Melinda enrolled in the Regent's Engineering Transfer program between Georgia Southern University and the Georgia Institute of Technology. She completed two years at GSU, before transferring to Georgia Tech pursuing a B.S. in Chemical Engineering. While in college, Melinda completed undergraduate research for the Polymer Manufacturing Research Center, focusing on post-consumer carpet recycling and polypropylene nanocomposites. After graduating in December 2002, Melinda began a position as a Product/Process Improvement Engineer for Milliken & Co. in the Automotive Division. At the Elm City Plant she has held two positions, the dyeing manager for Decorative Fabrics and the dyeing manager for Automotive Fabrics. Outside of work and school, Melinda enjoys watching football and basketball, bowling, and skiing in her free time.

**ACKNOWLEDGEMENTS**

I would like to thank Dr. Juan Hinestroza for all of his guidance and support in completing this project. Also I would like to thank Dr. Saad Khan and his research group for their help. Dr. Lei Qian and Dr. William Oxenham were also important members of my thesis committee. Dr. Carlos Rinaldi and his research group at the University of Puerto Rico at Mayaguez were very influential in the magnetic field experiments and magnetic characterization. Dr. Mark Walters and the Shared Materials Research Lab at Duke University provided training and support with different microscopy techniques. Dr. Gerardo Montero helped to train me on the electrospinning equipment and other analysis techniques. Finally, I would like to thank the Institute of Textile Technology and Milliken and Company for their financial support, career and research guidance.

## TABLE OF CONTENTS

**LIST OF FIGURES** ..... viii

**LIST OF TABLES** ..... xi

**1. INTRODUCTION** ..... 1

**1.1 BACKGROUND** ..... 1

**1.2 MOTIVATION** ..... 2

**1.3 OBJECTIVES** ..... 2

**2. LITERATURE REVIEW** ..... 3

**2.1 ELECTROSPINNING** ..... 3

**2.1.1 CONCEPT** ..... 3

**2.1.2 PARAMETER INVESTIGATION** ..... 6

**2.1.2.1 VISCOSITY** ..... 6

**2.1.2.2 CONDUCTIVITY** ..... 7

**2.1.2.3 SURFACE TENSION** ..... 8

**2.1.2.4 APPLIED ELECTRIC FIELD** ..... 9

**2.1.3 STABILITY ANALYSIS** ..... 10

**2.2 MAGNETIC NANOPARTICLES** ..... 11

**2.2.1 CONCEPT OF MAGNETISM** ..... 11

**2.2.2 MAGNETIC PROPERTIES** ..... 12

**2.2.3 FERROFLUIDS** ..... 15

**2.3 MAGNETIC FIELD EFFECTS** ..... 15

**2.4 FIBER ANALYSIS TECHNIQUES ..... 17**

**2.4.1 SCANNING ELECTRON MICROSCOPY ..... 17**

**2.4.2 TRANSMISSION ELECTRON MICROSCOPY ..... 17**

**2.4.3 MAGNETIC ANALYSIS/ SQUID ..... 19**

**3. EXPERIMENTAL PROCEDURE ..... 20**

**3.1 MATERIALS ..... 20**

**3.1.1 PREPARATION OF PEO-MAGNETITE SOLUTIONS ..... 20**

**3.1.2 VISCOSITY ..... 22**

**3.1.3 CONDUCTIVITY MEASUREMENTS ..... 23**

**3.1.4 SURFACE TENSION MEASUREMENTS ..... 24**

**3.2 ELECTROSPINNING EXPERIMENTS ..... 25**

**3.3 MAGNETIC FIELD EXPERIMENTS ..... 27**

**3.4 ANALYSIS METHODS ..... 28**

**3.4.1 SCANNING ELECTRON MICRCROSCOPY ..... 28**

**3.4.2 TRANSMISSION ELECTRON MICROSCOPY ..... 29**

**3.4.3 SUPERCONDUCTING QUANTUM INTERFERENCE DEVICE ..... 30**

**4. RESULTS AND DISCUSSION ..... 31**

**4.1 ELECTROSPINNING PHASE DIAGRAMS ..... 32**

**4.2 FIBER CHARACTERIZATION ..... 35**

**4.2.1 FIBER DIAMETER ..... 35**

**4.2.2 ENERGY DISPERSIVE SPECTROSCOPY ..... 41**

**4.3 MAGNETIC CHARACTERIZATION ..... 44**

**4.3.1 SQUID HYSTERESIS ..... 44**

**4.3.2 SQUID AC SUCEPTIBILITY ..... 47**

**4.4 ALTERNATING MAGNETIC FIELD ..... 49**

**5 CONCLUSIONS ..... 53**

**6 SUGGESTIONS FOR FURTHER RESEARCH ..... 54**

**7 REFERENCES ..... 58**

**APPENDICES ..... 63**

**APPENDIX A: CALCULATIONS ..... 64**

**APPENDIX B: VISCOSITY DATA ..... 67**

## LIST OF FIGURES

Figure 1 Main components of electrospinning set-up..... 4

Figure 2 Depiction of three phases of flow in electrospinning..... 5

Figure 3 Hysteresis curve example..... 14

Figure 4 Transmission microscope schematic [45] ..... 18

Figure 5 TEM micrograph of magnetite particles in the MSG W11 ferrofluid..... 21

Figure 6 Distribution histogram of magnetite particle size in MSG W11 ferrofluid..... 21

Figure 7 AR2000 Viscosity profiles for PEO/water, 0.01 v/v magnetite/ PEO, 0.10 v/v magnetite/PEO, and pure MSG W11 ferrofluid ..... 23

Figure 8 Conductivity Measurements for PEO/water, 0.01 v/v magnetite/ PEO, and 0.10 v/v magnetite/PEO..... 24

Figure 9 Surface tension measurements for PEO/water, 0.01 v/v magnetite/ PEO, and 0.10 v/v magnetite/PEO..... 25

Figure 10 NCSU laboratory electrospinning equipment ..... 26

Figure 11 Schematic of NCSU laboratory parallel plate electrospinning set-up..... 27

Figure 12 NCSU/UPRM laboratory electrospinning schematic with alternating magnetic field capabilities..... 28

Figure 13 Duke University Shared Materials Instrumentation Facilities Hitachi HF-2000 TEM..... 29

Figure 14 UPRM chemical engineering laboratory SQUID Magnetometer ..... 30

Figure 15 SEM micrograph of magnetite/PEO electrospun fiber web containing 0.01 v/v magnetite particles ..... 31

Figure 16 PEO/water electrospinning phase diagram depicting the flow rate and electric field for dripping, stable, and whipping flow ..... 32
Figure 17 Magnetite/ PEO (containing v/v 0.01magnetite) electrospinning phase diagram depicting the flow rate and electric field for dripping, stable, and whipping flow... 33
Figure 18 Magnetite/ PEO (containing v/v 0.10 magnetite) electrospinning phase diagram depicting the flow rate and electric field for dripping, stable, and whipping flow... 34
Figure 19 X-bar chart of electrospun magnetite/ PEO ( containing v/v 0.01magnetite) average fiber diameter..... 36
Figure 20 X-bar chart of electrospun magnetite/ PEO ( containing v/v 0.10magnetite) average fiber diameter..... 36
Figure 21 TEM micrograph of PEO nanofiber containing 0.01 v/v magnetite nanoparticles ..... 38
Figure 22 TEM micrograph of PEO nanofiber containing 0.01 v/v magnetite nanoparticles ..... 39
Figure 23 TEM micrograph of PEO nanofiber containing 0.10 v/v magnetite nanoparticles ..... 40
Figure 24 TEM micrograph of PEO nanofiber containing 0.10 v/v magnetite nanoparticles ..... 41
Figure 25 EDS spectrograph for PEO nanofiber containing 0. 01 v/v magnetite nanoparticles ..... 42
Figure 26 EDS spectrograph for PEO nanofiber containing 0. 10 v/v magnetite nanoparticles ..... 42

Figure 27 Room temperature hysteresis curve for electrospun PEO nanofiber containing 0.01 v/v magnetite nanoparticles ..... 45
Figure 28 Room temperature hysteresis curve for electrospun PEO nanofiber containing 0.10 v/v magnetite nanoparticles ..... 46
Figure 29 Out-of-phase component of the AC susceptibility for PEO nanofibers containing v/v 0.01 and v/v 0.10 magnetite nanoparticles..... 47
Figure 30 Out-of-phase component of the AC susceptibility for PEO nanofibers containing v/v 0.01 and v/v 0.10 magnetite nanoparticles..... 48
Figure 31 Electrospinning set-up #1 with AC magnetic field capabilities ..... 49
Figure 32 Electrospinning set-up #2 with AC magnetic field capabilities ..... 50
Figure 33 Electrospinning set-up #3 with AC magnetic field capabilities ..... 51
Figure 34 Backward Electrospinning Schematic ..... 52
Figure 35 Magnetite/ PEO (containing v/v 0.10 magnetite) electrospinning phase diagram depicting the flow rate and electric field for dripping, stable, and whipping flow using glass tip..... 55
Figure 36 Recommended solenoid enclosed in dielectric material for electrospinning with AC magnetic field ..... 56
Figure 37 TEM micrograph of PEO nanofiber containing 0.01 v/v functionalized magnetite nanoparticles ..... 57

## LIST OF TABLES

Table 1 Magnetite Particle Diameter Mean and Std. Deviation ..... 21

Table 2 Magnetite/ PEO volume fractions used in electrospinning trials ..... 22

Table 3 Hitachi HF-2000 Microscope settings ..... 29

Table 4 EDS summary for PEO nanofiber containing 0. 01 v/v magnetite nanoparticles 42

Table 5 EDS summary for PEO nanofiber containing 0. 10 v/v magnetite nanoparticles 43

# 1. INTRODUCTION

## 1.1 BACKGROUND

In recent years there has been increased interest in 'smart' materials that are sensitive to environmental changes and respond to external fields. These materials can alter their properties in response to changes in the surrounding environment. Of particular interest is the use of magnetic particles in combination with polymeric materials. The processiblity, noncorrosive nature, and light weight features of polymers make them excellent matrixes for magnetic particle inclusion. Magnetic nanoparticles can be embedded in polymeric matrices to impart the resulting nanocomposite with magnetic properties like unique AC susceptibility and hysteresis. For example, in the medical field, synthesizing drugs coated with magnetic nanocomposites provides a way for drugs to be released in a controlled manner using an external magnetic field [1]. Polymer nanocomposites have potential uses in producing magnetic recording media or high-frequency applications [2-4]. The magnetic responsiveness of these composites makes them of interest to the polymer, biomedical, and textile industries.

Electrospinning has been identified as a process able to produce polymeric fibers at the nanoscale level with nanoscale features. A better understanding of the operating parameters and solution parameters may help to de-bottleneck the electrospinning process and translate it from the laboratory to the commercial scale. The main research question of this work is: Can magnetic nanoparticles be used to improve the electrospinning

process and produce fibers with magnetic properties such as characteristic AC susceptibility spectra?

## 1.2 MOTIVATION

The production of fibers at the nanoscale level is of current interest to the textile industry. Polymer nanofibers have potential uses in protective clothing, 'smart clothing,' biomedical applications including would dressings and drug delivery systems, and anti-counterfeiting specialty fibers. The proposed research is expected to identify an alternative procedure to lower the viscosity of a polymer solution without lowering its concentration. In addition to de-bottlenecking the electrospinning process, the use of superparamagnetic particles can be used to develop fibers with controllable magnetic fingerprints. These fingerprints can aid in anti-counterfeiting devices and supply a 'signature' for the identification of textile raw materials and finished goods.

## 1.3 OBJECTIVES

1. To examine the factors that control final fiber diameter during the electrospinning process
2. To understand the effect of superparamagnetic particles on the solution properties and operating parameters of the electrospinning process
3. To examine nanofibers morphology and magnetic properties as a function of nanoparticle concentration

# 2. LITERATURE REVIEW

## 2.1 ELECTROSPINNING

### 2.1.1 CONCEPT

Electrospinning is a process able to generate fibers with diameters smaller than 200 nanometers. The concept of electrospinning is not new to the textile industry as the first patent dates back to the 1930s.With increased interest in smaller fibers, research efforts have concentrated on optimizing the electrospinning process for large-scale commercial production. As the knowledge base of the fundamentals of electrospinning expands, the solution viscosity has been identified as a key parameter in controlling the final fiber diameter [5-7]. The production of smaller fiber diameters often requires the use of dilute solutions and high power requirements, thereby limiting the production rate and commercialization of this process.

There are three major components in the electrospinning set-up: a high voltage power supply, a solution container connected to a conductive tip, and a metal collector [5]. The traditional process of electrospinning involves the application of high voltage to a capillary tip [5, 7]. The positive electrode is connected to the tip and the negative electrode connected to the collector [7].

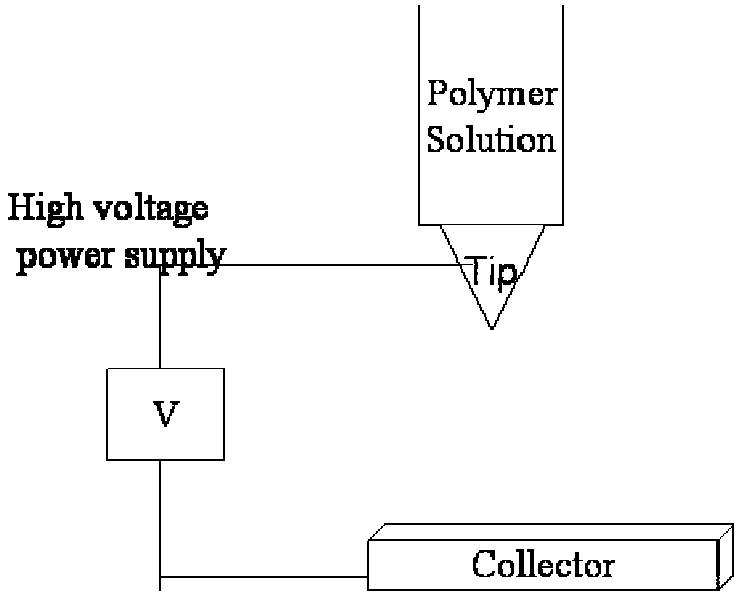


**Figure 1 Main components of electrospinning set-up**

The charged tip is connected to a polymer reservoir containing polymer solution. With the use of a pump, the polymer solution is fed through the tip into the electric field between the tip and the collector [7].

During the electrospinning process, a polymer solution is subjected to an electric field. When the surface tension of the solution is overcome by the charge induced by the electric field, a jet of polymeric solution is produced. As the jet leaves the tip, it takes on the shape of a Taylor cone [7, 8]. The jet proceeds in a straight line until it begins to bend in a zigzag pattern. During this time, the jet elongates, the solvent evaporates and polymer nanofibers on formed [9, 10].

The process of electrospinning begins as a polymer solution is pumped into a capillary and an electric field is created between the capillary and the collector. The electrical

forces elongate the jet of polymer solution, decreasing its diameter thousands or even millions of times. After the solvent evaporates, fibers with diameters in the range of 50 - 500 nanometers are then collected on an electrically grounded surface.

Unlike traditional fiber spinning techniques, electrospinning relies on electrical forces instead of mechanical forces [6]. These forces provide the phenomenon that transforms a drop into a jet as shown in Figure 1.

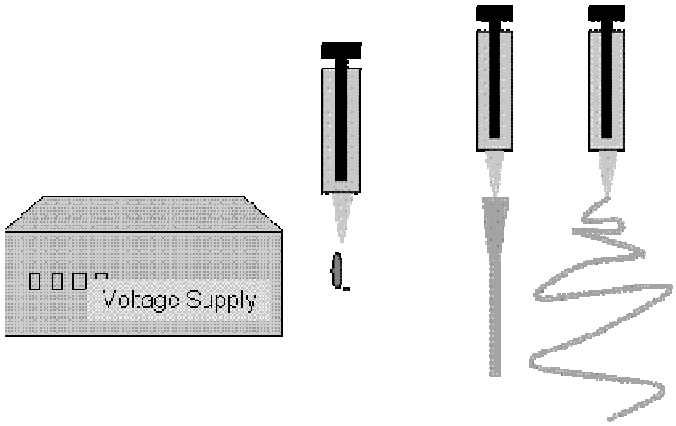


**Figure 2 Depiction of three phases of flow in electrospinning**

The jet thins as it heads toward the collector plate and it may experience a flow instability, known as whipping [11, 12]. This instability leads to extensive stretching and elongation of the jet. The whipping may decreases the fiber diameter up to 3 orders of magnitudes [13].

The electrostatic forces are not the only forces that affect the electrospinning process. Gravitational forces, columbic repulsive forces, viscoelastic forces, and surface tension all act on the charged jet [14]. The combination of these phenomena leads to different

trajectories for the jet. For example, the columbic repulsive forces contribute to the stretching of the jet, while the surface tension and viscoelastic forces act against it.

### 2.1.2 PARAMETER INVESTIGATION

As the investigation into the parameters that influence electrospinning nanofibers continues, the following properties have been identified as the most influential in controlling final fiber diameter: viscosity, conductivity, surface tension, and applied electric field.

#### 2.1.2.1 VISCOSITY

The viscous forces of a solution resist the electrical forces that attempt to stretch the fiber during electrospinning [15]. It has been found that there exists an optimum viscosity range for producing nanofibers [16]. At higher viscosities, the cohesiveness of the solution prohibits the formation of fibers [16, 17]. On the contrary, lower viscosities are more dilute and cause the production of droplets instead of fibers [5, 18, 19].

It is accepted that the viscosity of the polymeric solution influences the fiber diameter, and the concentration is proportional to the viscosity; therefore, several researchers have sought to establish relationships between the polymer concentration and the final fiber diameter. All data appears to support the idea that higher viscosity solutions produced fibers with larger diameters; however the disagreement occurs in developing a quantitative relationship between these two parameters [5, 14, 20]. Deitzel et al.

suggested that the there exists a power law relationship between the fiber diameter and the concentration [21]. Other researchers suggest a cubic power relationship between the final fiber diameter and the polymer concentration [5, 12]. Similarly, Mit-uppatham et al. proposed that for certain concentration ranges the average fiber diameter has an exponential relationship with concentration [14].

#### 2.1.2.2 CONDUCTIVITY

The conductivity of polymer solutions has also been identified as a key parameter in controlling the electrospinning process [13, 22, 23]. The conductivity of a solution describes the ability of a solution to carry an electrical current; therefore it affects the rate at which charge can move through a solution during electrospinning [22]. Some investigators have found that higher conductivity solutions created electrospun fibers with smaller diameters [24, 25]. The smaller diameters were attributed to higher charge density and increased fiber elongation.

However, some research supports the hypothesis that higher conductivity leads to larger fiber diameters. For example, Shin et al. found that higher conductivity solutions exhibited more stable fluid flow characteristics [26]. The increased stable flow led to less whipping instability; therefore fibers with larger diameters were formed. Also it was found that an increase in fiber diameter was sometimes observed when using solutions with higher conductivities due to salt addition [14]. Salts were usually added to polymer solutions because electricity passes easily through solutions with higher ion concentrations. An increase in the solution conductivity induces an increase in the

electrical shearing force during the electrospinning process. However this increase in fiber diameter was attributed to an increase in the viscosity due to the presence of the higher loads of salts [14]. Finally, Demir et al. observed that adding salts to increase the conductivity, did not have a significant effect on the fiber diameter [12].

#### 2.1.2.3 SURFACE TENSION

Surface tension is a measure of the cohesive forces between molecules in a liquid. Atoms on the surface of a solution prefer to be at the lowest energy state possible, so they configure themselves to minimize surface area, thereby lowering the number of available bonding sites on the surface. Molecules on the surface experience an attractive force towards the interior molecules, this is called surface tension. In electrospinning, this tension holds the solution droplet at the tip until the electric field provides enough force to overcome the surface tension [27].

Surface tension has also been identified as one of the key parameters in the electrospinning process [16, 23, 27]. A larger surface tension value signifies an increased difficulty in extending the surface of a liquid from the interior molecules. The surface tension is thought to be the force acting against the stretching of the charged jet; therefore higher surface tension leads to larger diameters [28].This claim was also supported by Wu et al., where it was found that lower surface tension samples produced thinner fibers [27]. In considering the three phases of electrospinning, higher surface tension is thought to act against the whipping instability [29]. Higher surface tension values favor a more stable jet flow, thereby creating fibers with larger diameters.

#### 2.1.2.4 APPLIED ELECTRIC FIELD

The electrical field is defined as the applied voltage divided by the distance between the tip and collector. Higher electric field values are obtained either through decreasing the distance between the tip and collector or by applying higher voltages. There exists controversy in the literature as to the effect of increasing the voltage on the final diameter of the electrospun nanofiber. According to Huang, it is found that an increase in the applied voltage leads to an increase in the fiber diameter due to the increase in the amount of fluid ejected [5]. On the contrary, Shin et al. states that as the electric field is increased, the jets thin more rapidly, leading to a smaller fiber diameter. This thinning was attributed to the jet being more unstable and the higher field creating more whipping oscillations [9, 26].

Doshi et al. observed that the jet diameter decreased with increasing distance between the tip and the collector [23]. It was suggested that the increased distance led to a larger amount of stretching of the jet before reaching the collector. Spivak et al. developed a model of steady state electrospinning to predict the final diameter of an electrospun fiber. The model took into account the inertial, hydrostatic, viscous, electric and surface tension forces of the system. The model agreed with the experimental results and indicated that the radius of the jet decreased with increasing distance from the capillary tip to the collector [6]. An increase in distance from tip to collector at a constant applied voltage, leads to a decrease in the electric field; therefore, the work of Doshi et al. and Spivak et al. suggest that the jet diameter decreases with decreasing electric field.

### 2.1.3 STABILITY ANALYSIS

Recent experimental observations have demonstrated that the thinning of a jet during electrospinning is mainly caused by the bending instability associated with the electrified jet [10, 30, 31]. At low field values, a single uniform fiber is reduced in size as it heads toward the collector. At higher field values the jet becomes unstable. Shin et al. pinpointed two modes of instability experienced during the electrospinning process. The first mode is varicose instability, where the centerline of the jet remains straight; while the radius of the jet changes. The second kind of instability is the whipping instability where the centerline of the jet is changing [26, 30]. The whipping mode provides the mechanism for nanofibers to occur. Controlling the transition between the instability modes can lead to new avenues to control the final fiber diameter. The studies of Shin et al. suggests that the growth of the 'whipping' region is the single most important factor in electrospinning [30].

Under the influence of an external electric field, the positive ions in a solution move toward the negative electrode in the electrospinning system. There exists a critical value where the potential difference is high enough that the electrical forces experienced by the jet overcome the surface tension, this value is known as the saturation value. Below the saturation value a stable jet appears, above this value instability occurs. Reneker et al. observed that the instability occurred in three repetitive phases. Stage one: smooth segments of the jet develop bends; stage two: each bended segment elongates and the loop size increases; stage three: the perimeter of the loops increase and the fiber diameter decrease [31].

## 2.2 MAGNETIC NANOPARTICLES

### 2.2.1 CONCEPT OF MAGNETISM

The spin of an electron along with orbital angular momentum are combined to create a magnetic dipole moment  Long range ordering of the spins of electrons creates regions known as magnetic domains [32]. In non-magnetic materials there is no long range order, because the spins of surrounding neighbors cancel each other out.

Magnetic materials can either be classified depending on their ability to be magnetized and the state of the material after the external magnetic field has been removed [33].  Soft magnets are materials that can be easily magnetized with a low strength external magnetic field and after the external source is removed these materials quickly return back to their original state. Of particular interest are paramagnetic materials, these are soft magnetic materials that possess high permeability and low resistance to orientation in the presence of an external field. Commonly used paramagnetic materials are iron, cobalt, nickel, and steel.

Materials that have atoms with permanent magnetic dipole moments are classified as either paramagnetic or ferromagnetic [32]. The difference between the two resides in the magnetic susceptibility of the material.  Ferromagnetic materials have permanent magnetic dipole moments that will align parallel to each other in a weak external field. The aligned moments, or domains will remain even after the external field is removed. In

the case of paramagnetic materials, it takes a stronger field to align the moments than that required by ferromagnetic materials and when the field is removed the moments are again randomly oriented. An extension of paramagnetism is superparamagnetism. Superparamagnetism and paramagnetism differ only in the fact that superparamagnetic materials are magnetized to a larger extent in moderate fields [34, 35]. These materials possess a high magnetic susceptibility.

The ability of magnetic domains to be aligned in the presence of an external field is the key in many technical applications for magnetic materials. The magnetic dipoles are randomly oriented normally, but in the presence of an external magnetic field, the particles can line up and orient in the direction of the applied field [36]. As the strength of the field increases, the material approaches a saturation point, which signifies the complete alignment of the dipoles [32]. The new field strength is equal to the applied field plus the contribution of the magnetic particles dipole moments.

### 2.2.2 MAGNETIC PROPERTIES

Magnetic materials are classified according to their permeability, coercivity, or hysteresis loss. Permeability is a measure of the degree of magnetization of a material when a field is applied. Coercivity is a measure of the strength of the field required to reduce a net magnetization to zero after a material has reached the saturation point, or the point where the material cannot absorb any more magnetization from the external source [33].

A hysteresis curve is a plot of magnetic flux density as a function of magnetic field strength. The hysteresis loop can reveal magnetic property information about the system. Ferromagnetic materials will reach a point where an increase in the external magnetic field strength, will not increase the magnetic flux density. This point is known as the saturation point. The magnetization of the material will depend on the history of the substance as well as the applied strength [32]. After an external source is removed, a remnant magnetization is present, so that the next time an external field is applied, the same field strength needed to reach the saturation point will be lessened due to the remnant magnetization. When this occurs, the material is said to possess hysteresis.

To understand the concept of paramagnetic particles consider a region where there exists a magnetic field $B_o$. If a magnetic substance is introduced into the region, the total magnetic field strength increases by the field produced by the magnetic substance [32]. The total magnetic field in the region becomes

$$B = B_o + \mu M \qquad (1)$$

Where μM is the contribution of the magnetic substance's moment. The total magnetic field strength is specified by a variable, H. This quantity is defined by the relationship

$$H = (B / \mu_0) - M \qquad (2)$$

For paramagnetic substances the magnetization M is proportional to the magnetic field strength H [34]. In these substances, one can write

$$M = \chi H \qquad (3)$$

Where χ is a dimensionless factor called the magnetic susceptibility.

The magnetic susceptibility of a material is the slope of the magnetization curve, or hysteresis loop.

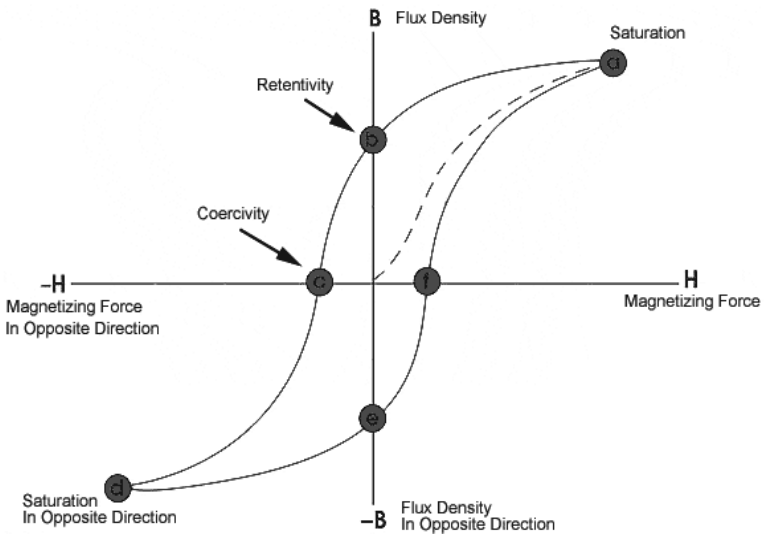


**Figure 3 Hysteresis curve example**

As shown in Figure 3, the magnetic flux (M) of a material increases as the magnetizing force increases (H), thereby showing the magnetization of the fibers. The magnetic flux continues to increase as the magnetic force increases until the saturation point, ($M_s$), is reached [37]. This point denotes the alignment of the majority of the domains; therefore, beyond this point, very little increase in the flux is accomplished by increasing the magnetizing force. The force H is reduced back down to zero, but the flux of the material has not returned back to zero. This point is a measure of the retentivity of the fiber ($M_r$). Finally the point where the flux returns to zero is a measure of the coercivity ($H_c$).

### 2.2.3 FERROFLUIDS

A ferrofluid is a special suspension of nanosized magnetic particles whose flow can be controlled by magnets or magnetic fields [38-40]. The magnetic fluids contain single magnetic domain particles coated with a dispersant and suspended in a liquid carrier. Brownian motion allows the particles to stay suspended and the surfactant layer prevents the particles from agglomeration [39]. The particles within this fluid have permanent magnetic dipole moments, exhibiting magnetic effects known as ferromagnetism. These substances have magnetic moments that align parallel to each other in the presence of an external magnetic field.

## 2.3 MAGNETIC FIELD EFFECTS

Paramagnetic substances have a positive but small magnetic susceptibility, or ability to become magnetized [32]. This ability is due to the presence of atoms with permanent dipole moments. These dipoles are oriented randomly in the absence of an external magnetic field. When the substance is placed in an external magnetic field, the dipoles tend to line up with the field [36, 38]. When a ferrofluid is exposed to an alternating magnetic field, each magnetic nanoparticle experiences a torque causing the particles and their surrounding fluid to spin [38]. Experimentally, it has been demonstrated that the nanoscale force resulting from the spinning of the nanoparticles can increase or decrease the effective magneto viscosity of the fluid [39-41].

Zeuner used magnetite based ferrofluids to prove that the viscosity of the magnetic fluid could be reduced by an alternating magnetic field. It was found that negative viscosities were experienced at higher frequencies and the effect became stronger as the frequency increased. The effect was documented at frequencies between 3005 Hz and 22321 Hz [41]. Rosenthal showed that a rotating spindle submerged in ferrofluid could be used to determine the effect of a magnetic field on the torque required to maintain a constant speed. These experiments varied the magnetic field amplitude and frequency to determine the required torque for speed consistency [42]. When the direction of the magnetic field was opposite the direction of the spindle, more torque was required. Less torque was required when the magnetic field direction was the same as the spindle rotation. This work showed the ferrofluids exerted a force on the surrounding fluid to create the negative viscosity effect.

An alternating magnetic field causes rotation of the magnetic particles but no direction is preferred [43]. The magnetic energy acts to power the angular momentum of the particles. If the field oscillates quick enough, or with a high enough frequency, the particles rotate quicker than the surrounding fluid. Bacri's work was in agreement with that of Zeuner in showing that the negative viscosity effect is a function of the frequency [43].

## 2.4 FIBER ANALYSIS TECHNIQUES

### 2.4.1 SCANNING ELECTRON MICROSCOPY

SEM uses the interaction of an electron beam with a sample to determine structural features [44]. A scanning electron microscope takes a diverging beam of electrons and converges it into a smaller beam using a series of lenses. The electron beam interacts with the top layers of a sample surface producing backscattered electrons, secondary electrons, and generated x-rays. The intensities of the secondary and backscattered electrons are used to develop an image of the sample based on the intensities of the electron events produced [44].

### 2.4.2 TRANSMISSION ELECTRON MICROSCOPY

Transmission electron microscopy relies on the transmission of electrons through a sample to create an image of the sample on a phosphor screen.

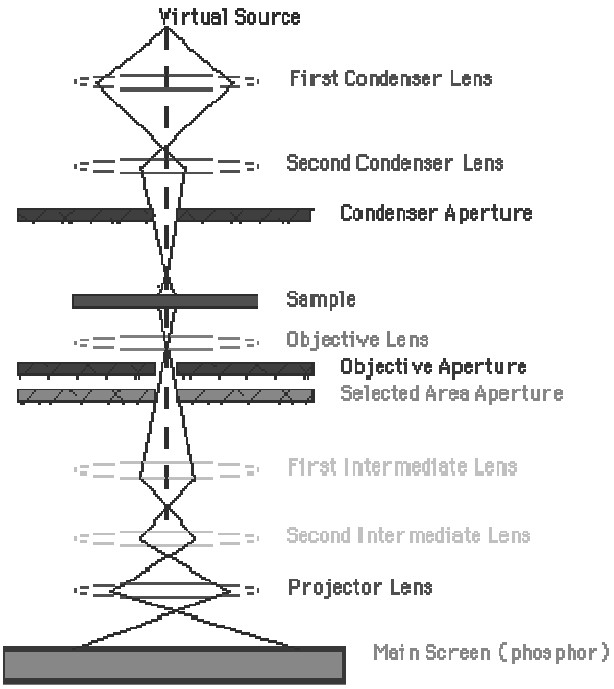


**Figure 4 Transmission microscope schematic [45]**

The TEM reveals information about sample morphology, crystallographic data using electron diffraction, and compositional analysis using energy dispersive or wavelength dispersive spectroscopy.

This technique has been used by many researchers including Kroell et al. to prove the homogeneity of magnetic domains inside a surrounding matrix material [46]. This technique can also be used to determine the average particles size, dispersion, and shape of nanoparticles in polymer matrices [47].

Elemental analysis is often combined with transmission electron microscopy by incorporating energy dispersive spectroscopy. By reducing the electron beam to a

nanometer spot size, the beam is intense enough to remove inner shell electrons from an electron orbital [44]. The inner shell electron is replaced by a higher shell electron and the differences in energy between the ejected and replacement electrons emit a characteristic x-ray. EDS can be used to determine the concentration of magnetic particles in a polymeric matrix [17]. Carpenter used this technology to determine the concentration of iron in an iron/gold based nanoparticle system [48].

### 2.4.3 MAGNETIC ANALYSIS/ SQUID

Superconducting quantum interference device (SQUID) has the ability to measure extremely small changes in the strength of a magnetic field. The SQUID measures the magnetic flux of a material as a function of an applied magnetic field [49].

SQUID analysis can provide information on the susceptibility, saturation, and coercivity of a sample[46, 50, 51]. Furthermore, an alternating current field can be applied and the flux generated by the sample detected. The flux is a measure of the response of a substance to an applied AC field. The change in flux as the field changes is called the AC susceptibility. Chi' ($\chi$') is a measure of the in-phase susceptibility of a material to a field and Chi'' ($\chi$'') is a measure of the out-of-phase component of the susceptibility.

# 3. EXPERIMENTAL PROCEDURE

## 3.1 MATERIALS

### 3.1.1 PREPARATION OF PEO-MAGNETITE SOLUTIONS

Polyethylene oxide (PEO) from Sigma-Aldrich with a molecular weight of 2,000,000 g/mol was used to prepare PEO solutions. 2 grams of PEO pellets were added to 100 ml of deionized water. The solution was stirred for 24 hours vigorously using a magnetic stirring rod.

Ferrofluids were added to the PEO solution. Ferrofluid type MSG W11, a water based suspension, produced by Ferrotec was used. This ferrofluid contained approximately 2.8-3.5 vol % magnetite ($Fe_3O_4$), 2-4 vol % dispersant and the remaining solution was water. Some of the properties of the ferrofluid include: saturation magnetization 0.0203 Tesla, low field magnetic susceptibility $\lambda = 0.65$, mass density 1204 $kg/m^3$

Using transmission electron microscopy, the average magnetite particle size was found to be 13.5 nm as shown in Table 1.

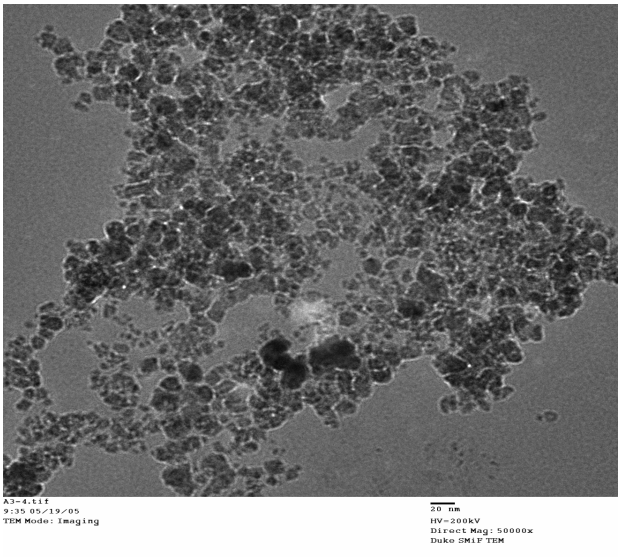


**Figure 5 TEM micrograph of magnetite particles in the MSG W11 ferrofluid**

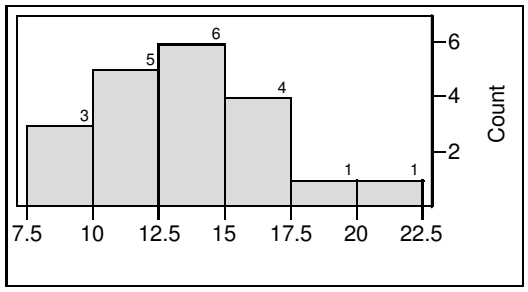


**Figure 6 Distribution histogram of magnetite particle size in MSG W11 ferrofluid**

**Table 1 Magnetite Particle Diameter Mean and Std. Deviation**

| | |
|---|---|
| **Mean** | **13.5 nm** |
| **Std Dev** | **3.44 nm** |
| **Sample Size** | **20** |

The nanoparticle diameters ranged from 7.5 nm to 22.5 nm.

A low and a high level loading of magnetite was selected, v/v 0.01 and v/v 0.10 respectively for the electrospinning solutions. Appendix A describes the calculations used to determine the amount of ferrofluid needed to achieve the desired concentrations. The calculations were based on the assumption that all of the water evaporates leaving only PEO and magnetite in the resulting nanofiber.

**Table 2 Magnetite/ PEO volume fractions used in electrospinning trials**

| SAMPLE | Vol. PEO/Water (ml) | Particle V/V (fiber) | Ferro Vol (ml) | Particle Vol (ml) | Particle V/V (solution) |
|---|---|---|---|---|---|
| 1 | 20 | 0.01 | 0.10 | 0.0034 | 0.0002 |
| 2 | 20 | 0.1 | 1.08 | 0.0389 | 0.0018 |

### 3.1.2 VISCOSITY

An AR2000 rheometer (TA Instruments) was used to perform viscosity measurements of the solutions. The concentric cylinder geometry was used to measure the stress and strain profile of the pure PEO/water solution, electrospinning solutions, and the profile of the pure ferrofluids. The Rheology Advance Instrument Control software was used to analyze the viscosity data. Figure 7 illustrates the viscosity profiles of the four solutions.

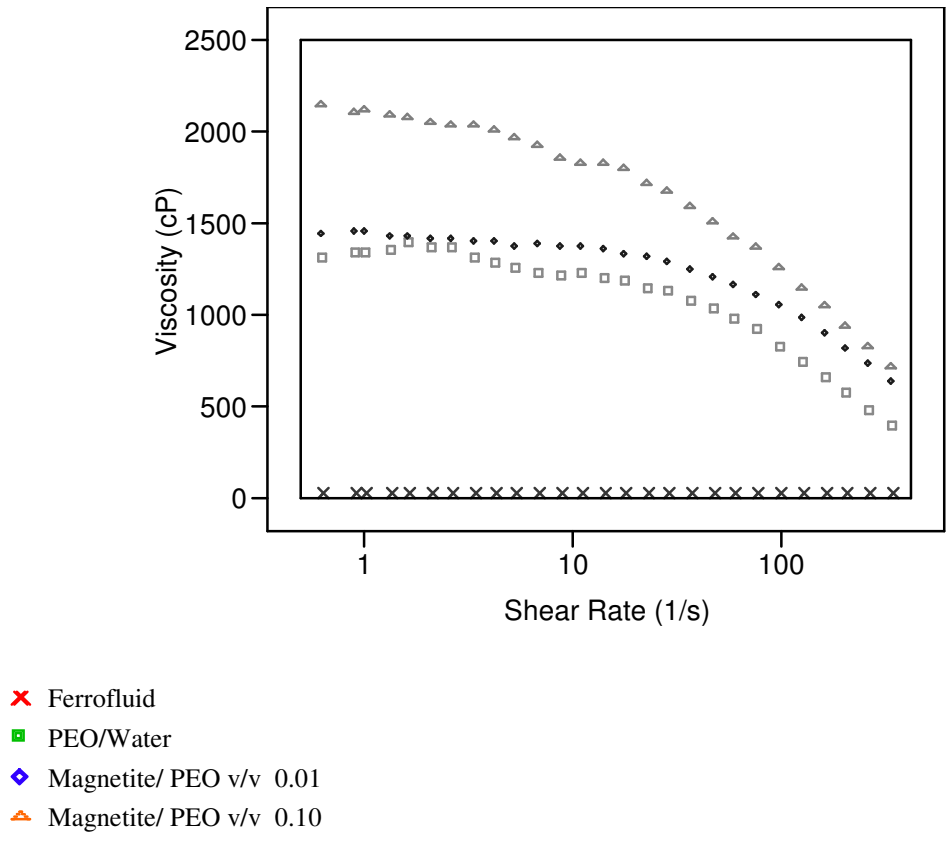


**Figure 7 AR2000 Viscosity profiles for PEO/water, 0.01 v/v magnetite/ PEO, 0.10 v/v magnetite/PEO, and pure MSG W11 ferrofluid**

The viscosity of the PEO/water solution increased with increasing magnetite concentration.

### 3.1.3 CONDUCTIVITY MEASUREMENTS

Conductivity Measurements were performed using a conductivity meter (Thermo) Orion 162A. 30ml aliquots of the PEO/water solution, PEO/magnetite (v/v 0.01), and PEO/magnetite (v/v 0.10) were used for the conductivity measurements. The accuracy of the meter is 0.5%.

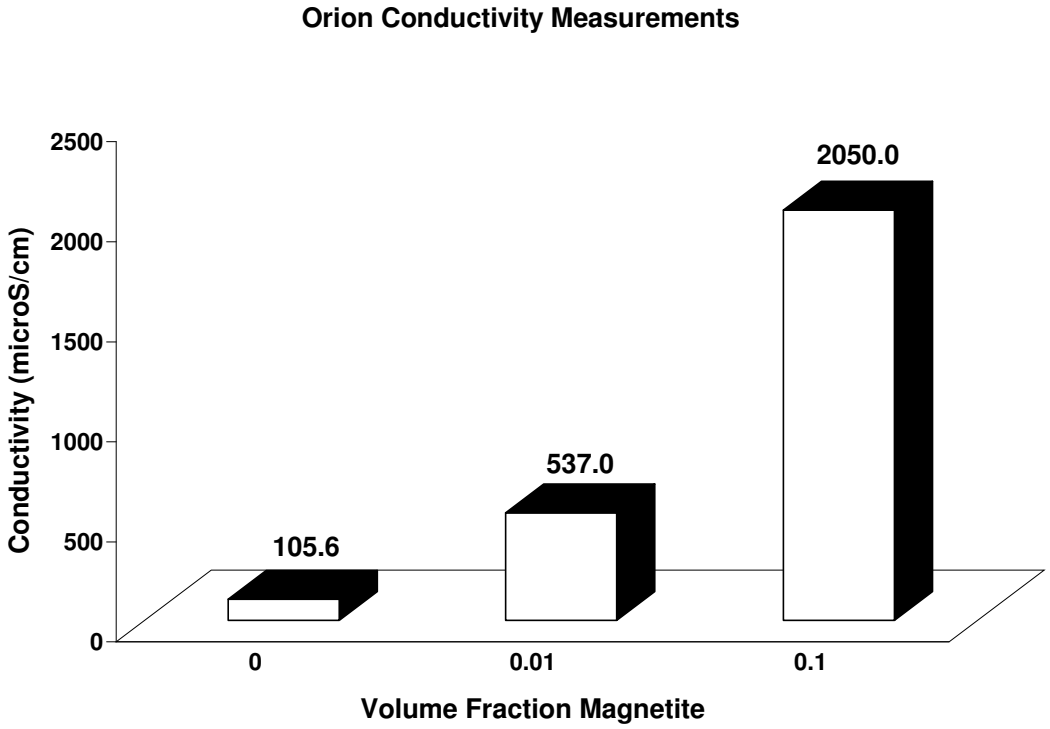


**Figure 8 Conductivity Measurements for PEO/water, 0.01 v/v magnetite/ PEO, and 0.10 v/v magnetite/PEO**

Figure 8 shows how increasing the loading of magnetite, increased the conductivity of the electrospinning solutions.

### 3.1.4 SURFACE TENSION MEASUREMENTS

Surface tension measurements were performed using the Fisher Tensiomat Model 21. A platinum-iridium ring was used. The force required to pull the ring out of the samples was measured in dynes/cm. Normal laboratory temperature and humidity were used for these measurements. Three repetitions of each measurement were performed and the average of the measurements is shown in Figure 9.

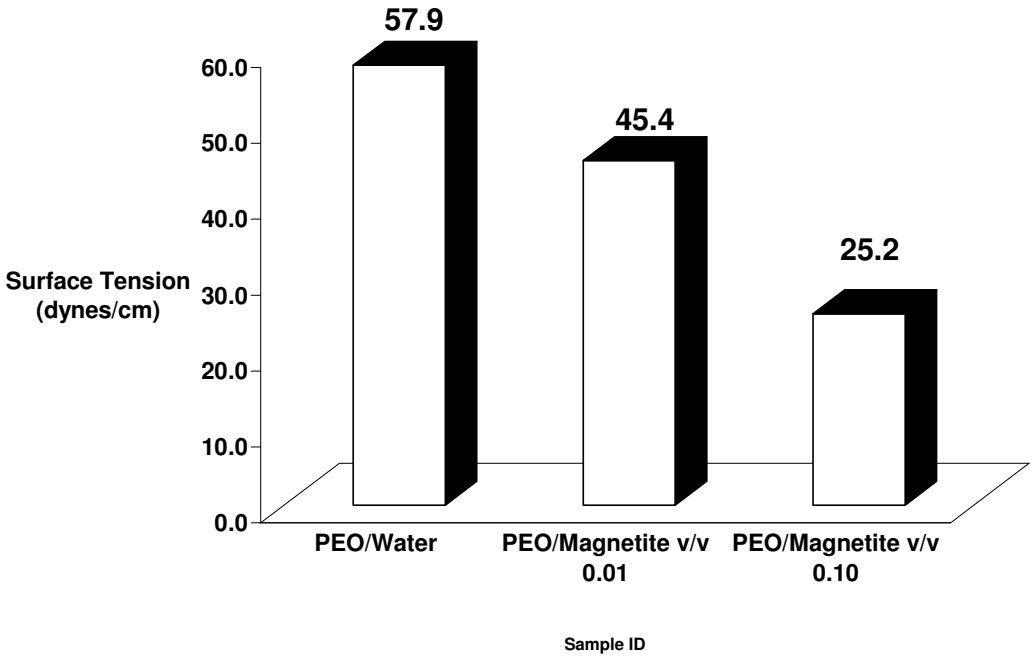


**Figure 9 Surface tension measurements for PEO/water, 0.01 v/v magnetite/ PEO, and 0.10 v/v magnetite/PEO**

The inclusion of the magnetite particles produced a decrease in the PEO/water solution surface tension.

## 3.2 ELECTROSPINNING EXPERIMENTS

A parallel plate electrospinning apparatus was used to supply a uniform electric field for the trials. Two aluminum plates with diameters of 12 inches were vertically aligned with the distance between the two plates ranging from 15 cm- 25 cm. The solutions were pumped at a specific flow rate using the NE 500 micro diaphragm pump by New Era Pump Systems controlled by Pumpterm software. The solution reservoir was a 60 ml

plastic syringe that was connected to the capillary tip using C-flex tubing with an inner diameter of 0.125 inches. An electrical potential was applied using a Series EL DC High Voltage power supply made by Glassman.

The plates were enclosed in a plastic enclosure. The bottom plate was positioned on an adjustable lift that was used to set the plate to plate distance. The top plate had a 5 mm hole in center of the plate to serve as the capillary tip entry point. The tip was aluminum with an inner diameter of 0.75 mm and an outer diameter of 4 mm.

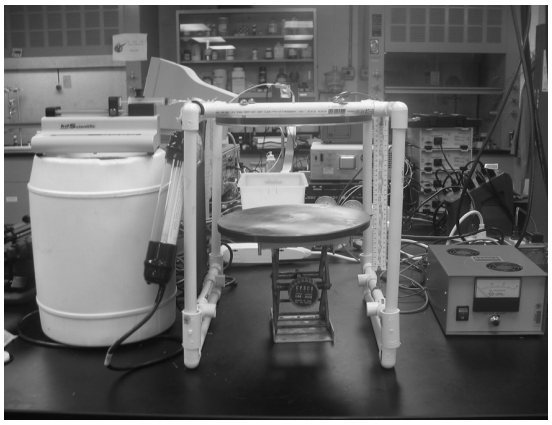

**Figure 10 NCSU laboratory electrospinning equipment**

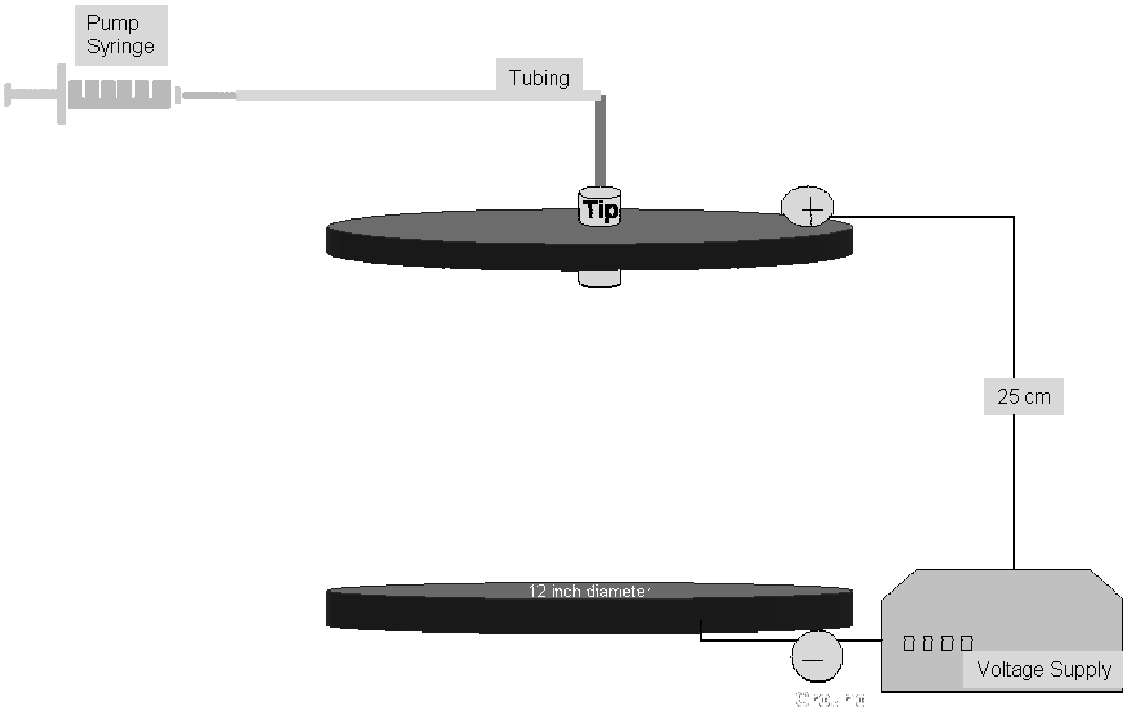


**Figure 11 Schematic of NCSU laboratory parallel plate electrospinning set-up**

## 3.3 MAGNETIC FIELD EXPERIMENTS

The magnetic field was supplied using an AC power supply connected to a solenoid of magnetic wire. The solenoid had 30 turns of 13 gauge (1.8 mm diameter) copper magnet wire. A Wavetek 2 MHz Sweep/Function Generator Model 19 was used to generate sine wave functions. An AE Techron 5050 Linear Amplifier was used in conjunction with the Wavetek Function Generator to supply alternating current. A glass capillary tip was used with inner diameter of 1.5 mm. The solenoid was placed on the top plate and it surrounded the glass capillary so that the magnetic field force would be downward towards the capillary tip, as shown in Figure 11.

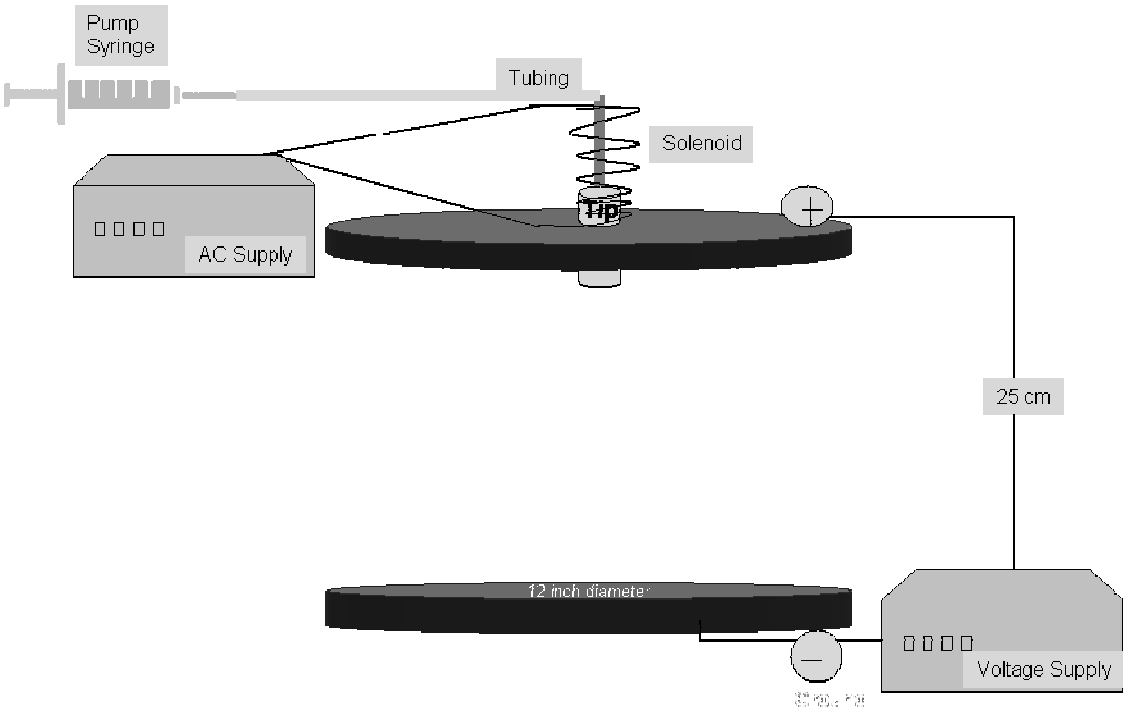


**Figure 12 NCSU/UPRM laboratory electrospinning schematic with alternating magnetic field capabilities**

## 3.4 ANALYSIS METHODS

### 3.4.1 SCANNING ELECTRON MICRCROSCOPY

A Hitachi SN 3200 variable pressure scanning electron microscope was used to retrieve high resolution images of the fiber webs after electrospinning. The accelerating voltage used varied from 0.3 kV- 30 kV with a working distance of 3-60 mm. The samples were directly deposited on to aluminum foil during electrospinning. The fiber webs were sputter coated with gold prior to imaging to prevent charging.

### 3.4.2 TRANSMISSION ELECTRON MICROSCOPY

A Hitachi HF-2000 Transmission Electron Microscope was used to analyze the fiber size and particle distribution.

**Figure 13 Duke University Shared Materials Instrumentation Facilities Hitachi HF-2000 TEM**

The fibers were directly deposited onto 3 mm mesh copper TEM grids. The following parameters were used as standard operating procedures.

**Table 3 Hitachi HF-2000 Microscope settings**

| Accelerating Voltage (kV) | Beam Current (micro A) | Column Pressure (Pa) | Voltage Ratio | Magnification Range used |
|---|---|---|---|---|
| 200 | 30 | <10-5 | 5.5 | 10-100, 000X |

The HF-2000 is also equipped with a silicon x-ray detector for energy dispersive spectroscopy. The analysis software used was INCA for elemental identification of the characteristic x-rays produced.

### 3.4.3 SUPERCONDUCTING QUANTUM INTERFERENCE DEVICE

A superconducting quantum interference device (SQUID) was used to determine the magnetic response of the fibers to an applied AC field. The Quantum Design MPMS-XL7 SQUID magnetometer was used to determine the hysteresis behavior and the AC out of phase component of the susceptibility of the fibers.

**Figure 14 UPRM chemical engineering laboratory SQUID Magnetometer**

Using the SQUID magnetometer, the susceptibility was measured as a function of the AC field frequency.

## 4. RESULTS AND DISCUSSION

The values of the flow rate, applied voltage, plate to plate distance, and capillary tip size were preliminarily screened to determine the operating parameters that would allow whipping to occur. When whipping occurred PEO/magnetite fiber webs were formed and collected on the bottom collector plate. Scanning electron microscopy was used to examine the fibers.

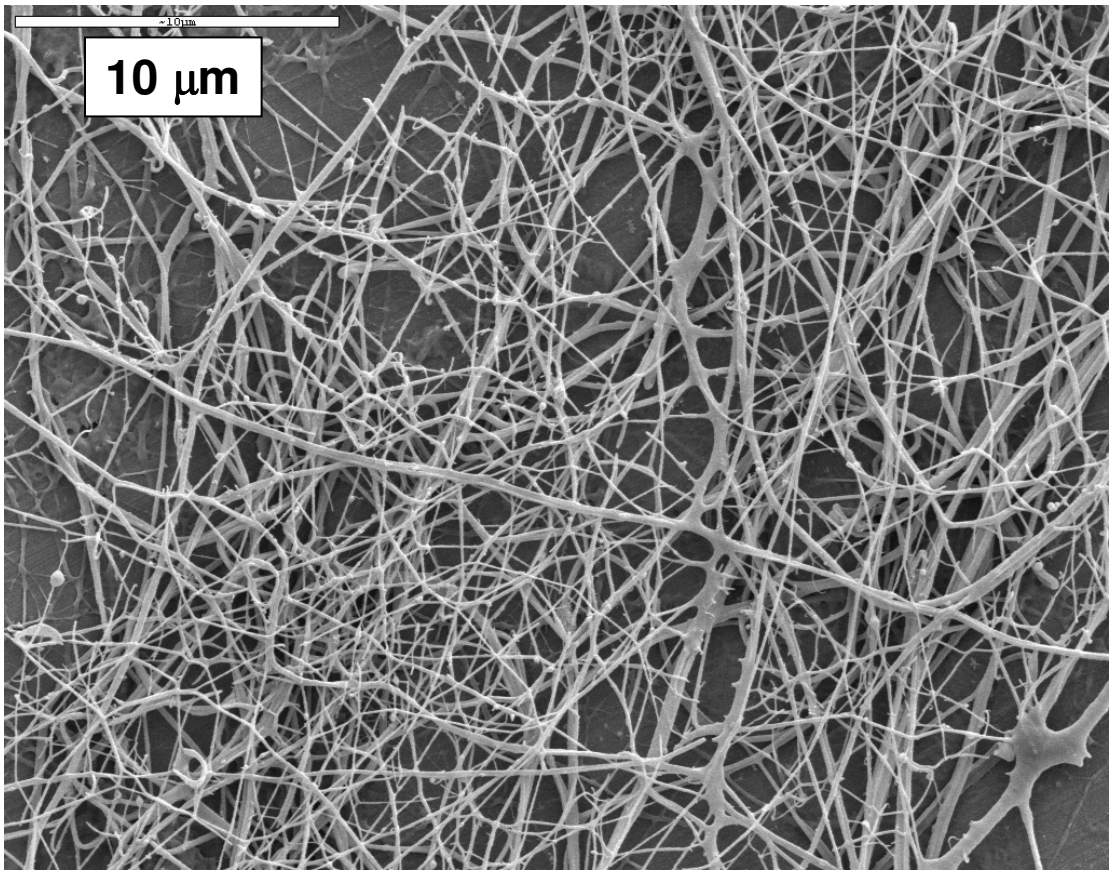


**Figure 15 SEM micrograph of magnetite/PEO electrospun fiber web containing 0.01 v/v magnetite particles**

## 4.1 ELECTROSPINNING PHASE DIAGRAMS

Phase diagrams of three different solutions were developed: 2wt% PEO/water, PEO solution with v/v 0.01 $Fe_3O_4$, and PEO solution with v/v 0.10 $Fe_3O_4$. The change in jet flow was observed by lowering the laboratory lights and using a strobe lamp to illuminate the electrospinning jet. The phase diagrams were completed to determine the electric field and flow rate where dripping, stable flow, and whipping flow existed for each of the three solutions. The electric field range was 0.4 kV/cm - 2 kV/cm and the flow rate range tested was 0.1 ml/min to 0.3 ml/min.

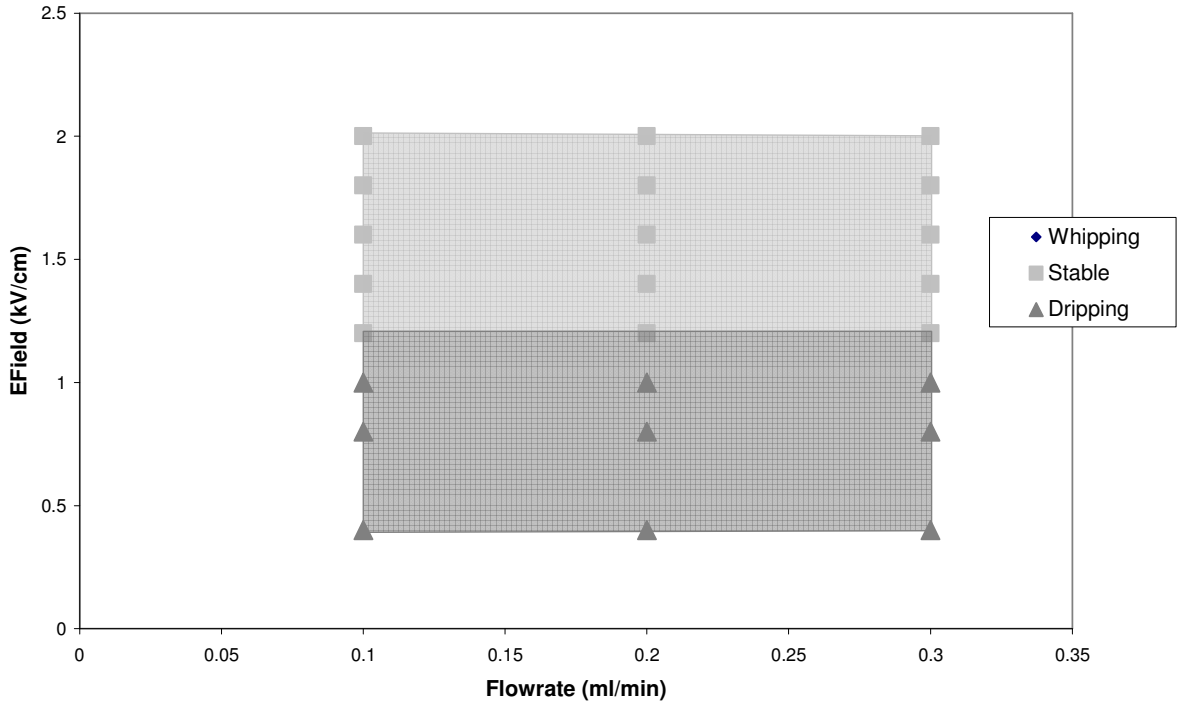


**Figure 16 PEO/water electrospinning phase diagram depicting the flow rate and electric field for dripping, stable, and whipping flow**

To transition from dripping to stable, an electric field of 1.25 kV/cm was required at all flow rates. For pure PEO/water, the dripping and stable region were observed, but no whipping phase was observed. Other researchers observed whipping phases in PEO/water solutions; however, the solutions usually contained salts to increase the electrostatic forces that promote whipping [9].

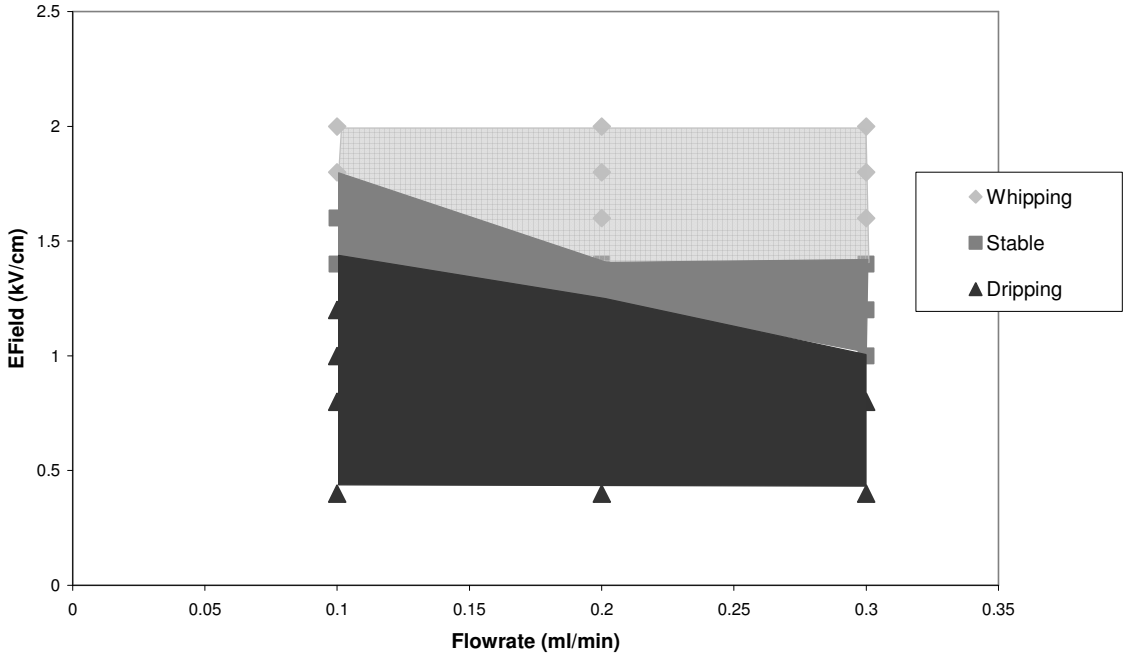


**Figure 17 Magnetite/ PEO (containing v/v 0.01magnetite) electrospinning phase diagram depicting the flow rate and electric field for dripping, stable, and whipping flow**

For the PEO/water solution containing v/v 0.01 of magnetite, lower flow rates required a higher field value to transition from dripping to stable than higher flow rates. In comparison to pure PEO/water, the inclusion of the magnetite particles provided solution parameters conducive for whipping instability.

Figure 18 illustrates a phase diagram for the PEO solutions containing v/v 0.10 of magnetite. As with the v/v 0.01 solution, whipping occurred at field values between 1.6 - 1.8 kV/cm.

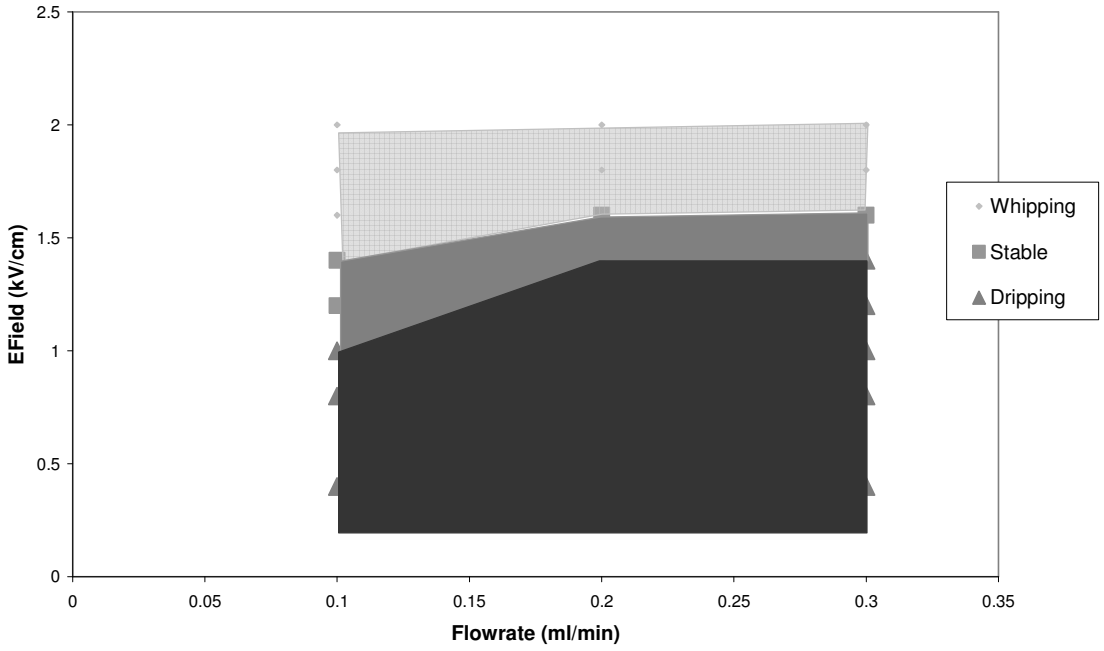


**Figure 18 Magnetite/ PEO (containing v/v 0.10 magnetite) electrospinning phase diagram depicting the flow rate and electric field for dripping, stable, and whipping flow**

Several differences can be noted between the phase diagrams for the two solutions. Lower applied fields were required to transition from dripping to stable for the solution containing higher loads of magnetite. This difference may be attributed to the decrease in surface tension. Lower surface tension implies a lower cohesiveness of the droplet; therefore it is easier to transition from dripping to stable. Secondly, the shape of the transition curves differed for the two solutions. The higher magnetite concentration

solution behaved more like solutions in the literature [9]. At higher flow rate, the fluid carries less negative charge as it is headed toward the positive electrode; thereby requiring higher field values at higher flow rates. The charge per unit volume is lower with increasing flow rate; thereby higher fields are required for higher flow rates.

In evaluating the effects of the magnetite inclusion, it was shown that the magnetic nanoparticles created solution properties favorable for whipping instability. The solution containing higher loadings of magnetite had a higher conductivity, higher viscosity, and lower surface tension. The magnetic particles lowered solution surface tensions and increased conductivities to promote the transition from stable to whipping. . It was observed that the whipping oscillations were more vigorous for the solution containing more ferrofluid. The inclusion of the magnetite particles fashioned properties conducive for nanofiber production.

## 4.2 FIBER CHARACTERIZATION

### 4.2.1 FIBER DIAMETER

Transmission electron microscopy was used to observe the fiber shape and size distribution. Twenty fibers were measured to determine the average diameter size of the fibers and the range of fiber sizes. Three measurements were taken of each fiber using Image Tool software. The average diameter of the three measurements was plotted on a x-bar chart using Jump software.

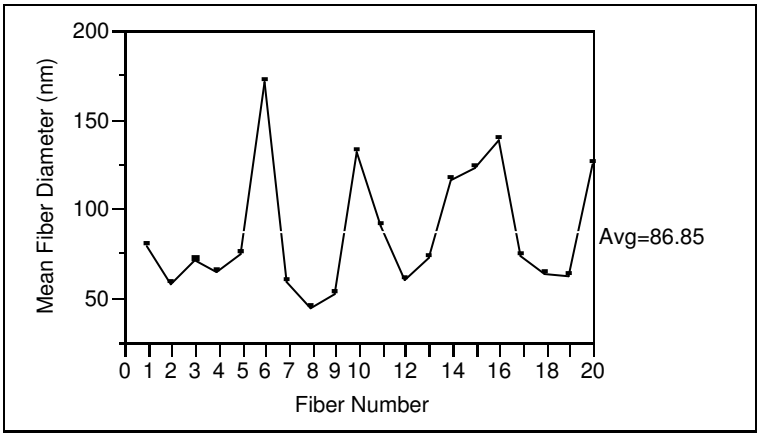


**Figure 19 X-bar chart of electrospun magnetite/ PEO ( containing v/v 0.01magnetite) average fiber diameter**

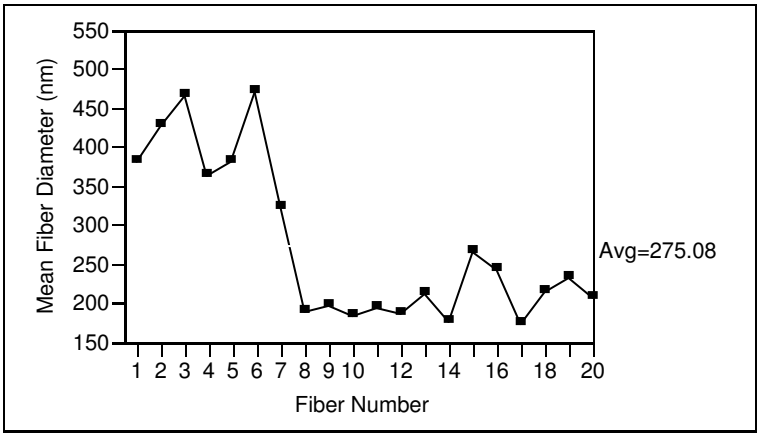


**Figure 20 X-bar chart of electrospun magnetite/ PEO ( containing v/v 0.10magnetite) average fiber diameter**

The average diameter for the solutions having higher ferrofluids concentration (v/v 0.10) was 275 nm in comparison to an average diameter of 87 nm for the lower concentration solution. Including the variation in the diameter sizes, there was a statistical difference between the two values. The higher magnetite loadings led to a larger fiber diameter. The operating parameters e.g. plate to plate distance, flow rate, tip size were the same for

both solutions. The difference exists in the solution parameters. The higher conductivity solution and higher viscosity produced fibers with larger diameters. The solution surface tension was lower, but the effect of the surface tension was outweighed by the effect of the viscosity. Whipping occurred with an applied field of 1.8 kV in both cases, however the higher loading solution produced fibers that were elongated less during the whipping process.

Using transmission electron microscopy images of the PEO/magnetite fibers were obtained. Fibers were deposited directly onto the TEM micrograph grids while whipping occurred during the electrospinning process. Figures 21 and 22 are micrographs of PEO fibers with v/v 0.01 loading of magnetite.

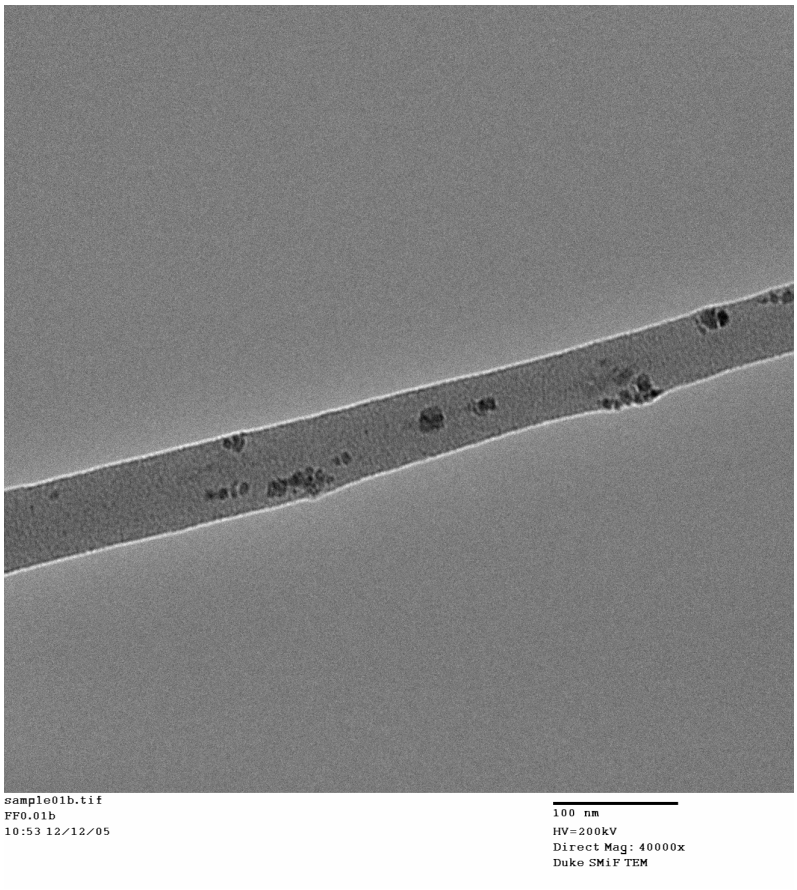


**Figure 21 TEM micrograph of PEO nanofiber containing 0.01 v/v magnetite nanoparticles**

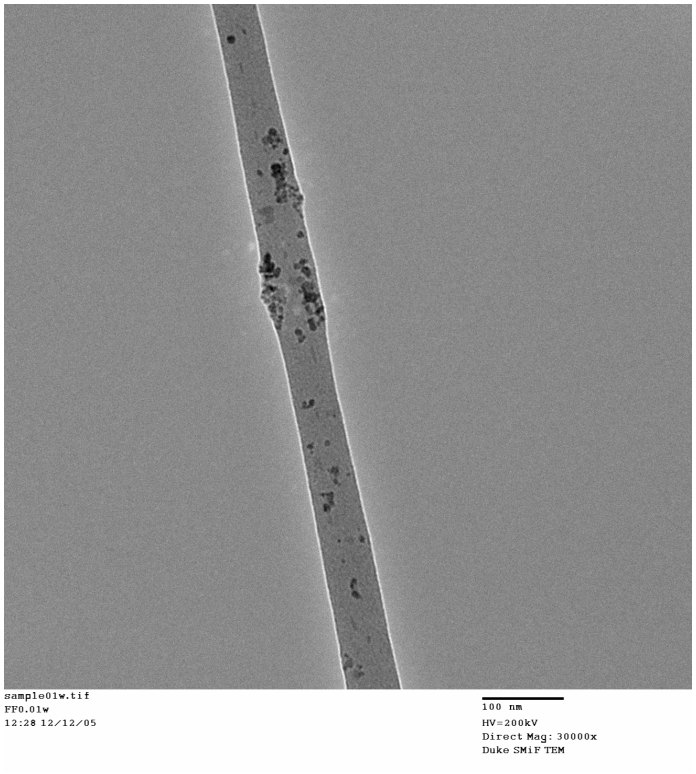


**Figure 22 TEM micrograph of PEO nanofiber containing 0.01 v/v magnetite nanoparticles**

The dark regions in these fibers correspond to the magnetite nanoparticles dispersed within the polyethylene oxide matrix. The micrographs show some particle agglomeration within the fibers. The agglomeration could be attributed to the mixing process during the preparation of the spinning solutions, or settling of the particles from the polymer solution.

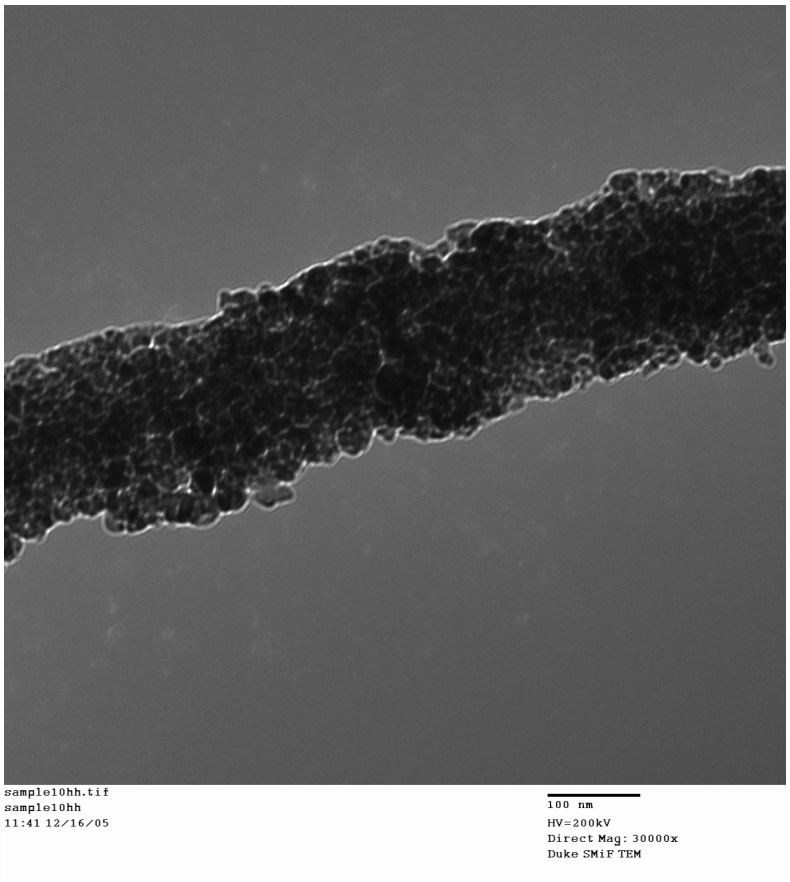


**Figure 23 TEM micrograph of PEO nanofiber containing 0.10 v/v magnetite nanoparticles**

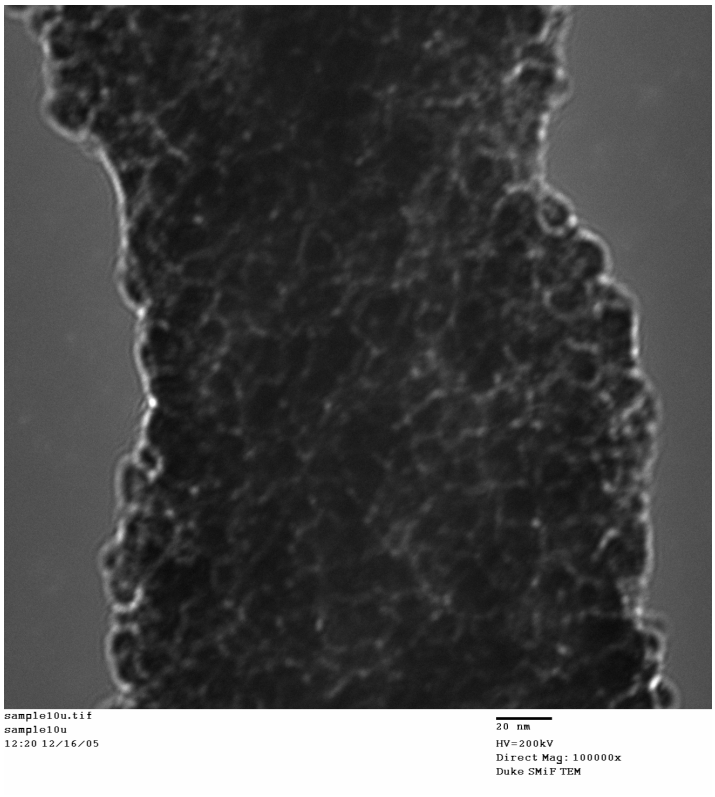


**Figure 24 TEM micrograph of PEO nanofiber containing 0.10 v/v magnetite nanoparticles**

Figures 23 and 24 are micrographs of the fibers containing 0.10 v/v magnetite particles. From these micrographs it can be seen that the fibers containing larger magnetite loading were concentrated with nanoparticles in comparison to the randomly dispersed particles seen in the lower concentration fibers.

### 4.2.2 ENERGY DISPERSIVE SPECTROSCOPY

Energy dispersive spectroscopy was used to identify the elements present in the fibers analyzed. The characteristic x-rays for iron, carbon, and oxygen were identified in all samples. This quantitative analysis showed an increase in the relative intensities of the iron as the percent magnetite increased in the fibers.

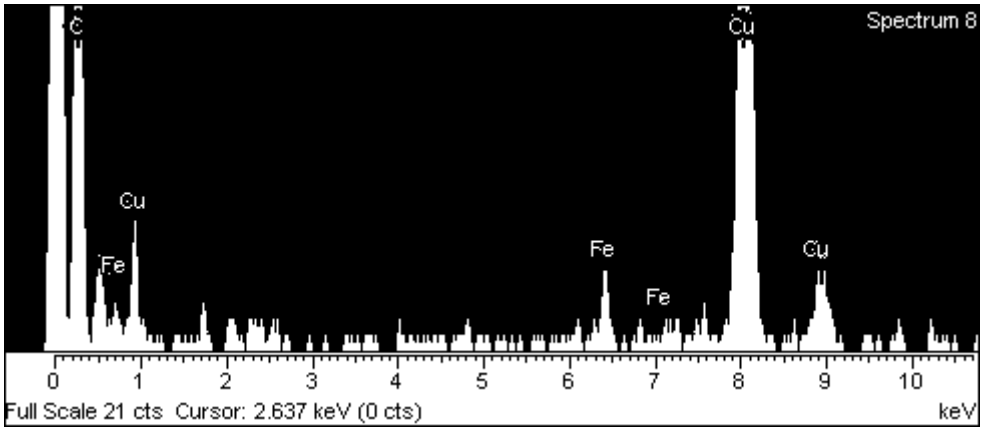


**Figure 25 EDS spectrograph for PEO nanofiber containing 0. 01 v/v magnetite nanoparticles**

**Table 4 EDS summary for PEO nanofiber containing 0. 01 v/v magnetite nanoparticles**

| Element | Weight % |
|---|---|
| Carbon | 94.4 |
| Iron | 5.6 |

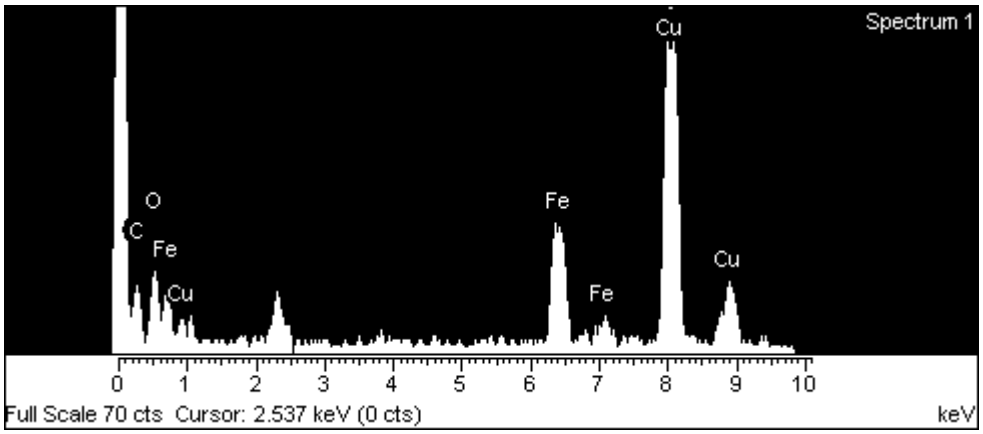


**Figure 26 EDS spectrograph for PEO nanofiber containing 0. 10 v/v magnetite nanoparticles**

**Table 5 EDS summary for PEO nanofiber containing 0. 10 v/v magnetite nanoparticles**

| Element | Weight % |
|---|---|
| Carbon | 15.7 |
| Oxygen | 25.5 |
| Iron | 58.8 |

The iron K- alpha peak was identified in all samples at 6. 40 keV, the higher energy K-beta peak was found at 7.06 keV. The iron L-series peaks were not resolved into individual peaks, but combined into one peak at 0.71 keV. The K- alpha peak of oxygen was identified at 0.52 keV. K and L denote the shells from which the electrons were removed. Alpha transitions occur when an electron moves from L shell to the K shell; beta transitions occur when an electron moves from the M shell to the K shell.

Oxygen is present in the polyethylene oxide matrix but also in the magnetite crystal structure. At higher magnetite levels, the oxygen produced a more prominent and intense spectra. Carbon's K-alpha peak at 0.28 keV was found in both samples.

The weight percent of iron in the samples increased from 5.6% for v/v 0.01 of magnetite fiber to 58.83 % for v/v 0.10 magnetite fibers. In Appendix A, calculations are shown that determine the weight percent magnetite in the final fiber. The calculations predicted that polyethylene nanofibers containing v/v 0.01 magnetite would have 4.5 wt% magnetite. This designed value is similar to the 5.6% predicted by EDS. Also it was calculated that the polyethylene nanofibers containing v/v 0.10 magnetite particles would have 45.6 wt% magnetite. The differences in the EDS estimated value and the calculated values reside in the fact that EDS must be calibrated using a standard to exactly quantify weight percentages.

During analysis of the 0.10 v/v magnetite fiber, the existence of a sulfur k-alpha peak was identified. This peak was attributed to the surfactant layer of the ferrofluids. The copper peak identified is due to the copper grid that the fibers were deposited on for TEM analysis.

## 4.3 MAGNETIC CHARACTERIZATION

### 4.3.1 SQUID HYSTERESIS

The hysteresis curve revealed the magnetic properties of the fibers. The saturation point, $M_s$, the amount of magnetization retained, $M_r$, and the coercivity $H_c$ of the fibers are all denoted on the hysteresis curves.

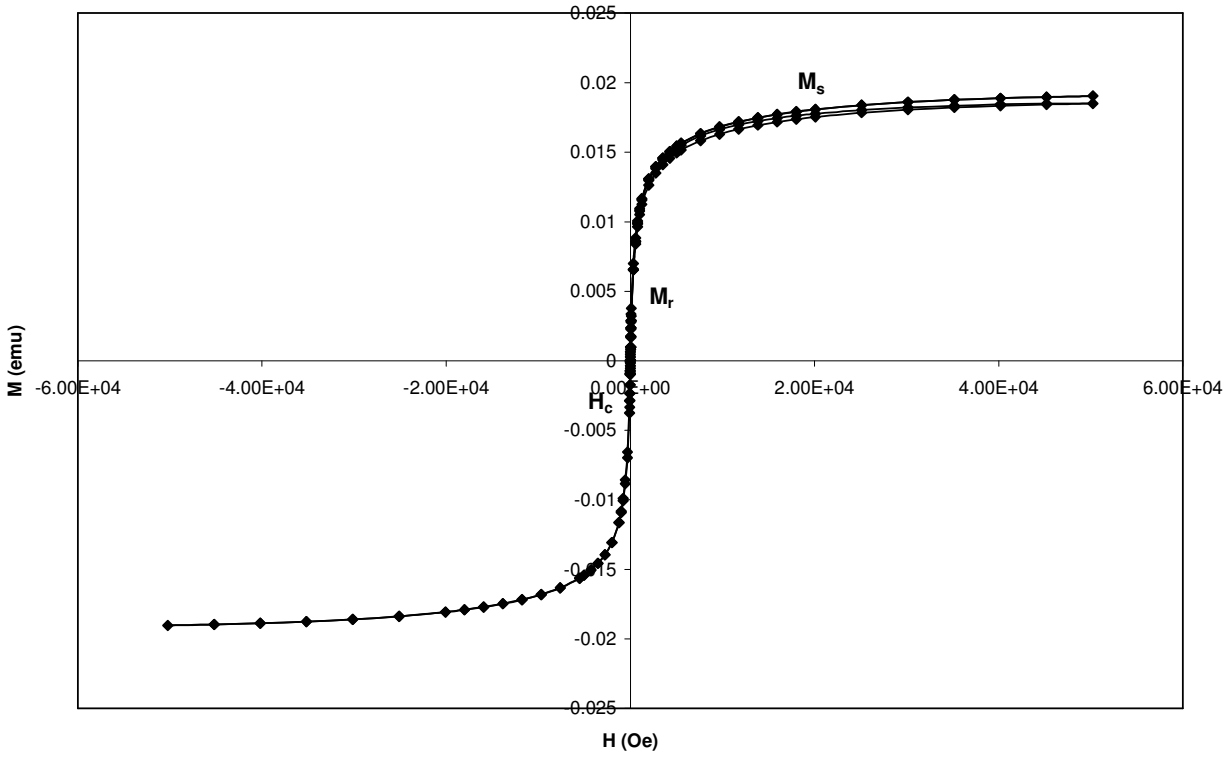


**Figure 27 Room temperature hysteresis curve for electrospun PEO nanofiber containing 0.01 v/v magnetite nanoparticles**

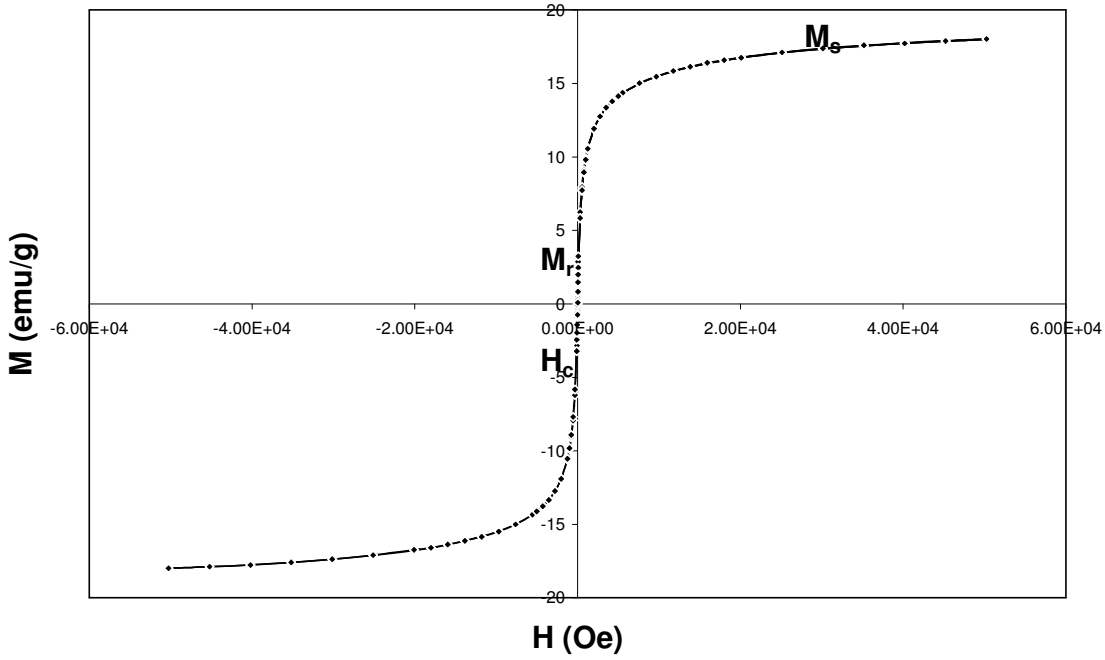


**Figure 28 Room temperature hysteresis curve for electrospun PEO nanofiber containing 0.10 v/v magnetite nanoparticles**

In Figures 27 and 28, it can be observed that the saturation magnetization increases with increasing magnetite concentration. This is due to the fact that those fibers contained more domains to contribute to the magnetic flux. The TEM micrographs of the fibers with the lower concentration of ferrofluids showed clustering of particles. The clusters of particles act to cancel out the magnetic moments of the surrounding particles; thereby reducing the contribution of the particles to the magnetic flux.

The remnant magnetization of the lower concentration fiber was 0.0241 emu/g in comparison to 0.0811 emu/g for the higher loading fiber sample. The remnant magnetization was higher for v/v 0.10 fiber than for the v/v 0.01 fiber, signifying that

after the applied field was removed, more domains remained aligned in the fiber containing the higher concentration magnetite.

### 4.3.2 SQUID AC SUCEPTIBILITY

Figure 29 shows the out-of-phase component of the AC susceptibility for the two samples of fibers.

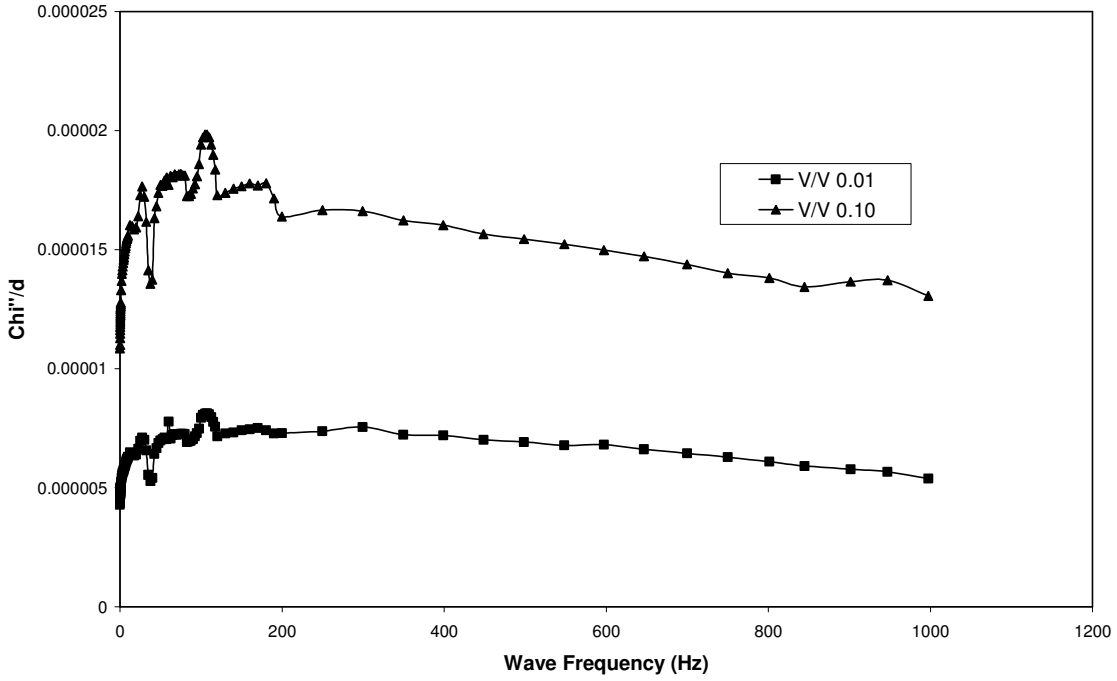


**Figure 29 Out-of-phase component of the AC susceptibility for PEO nanofibers containing v/v 0.01 and v/v 0.10 magnetite nanoparticles**

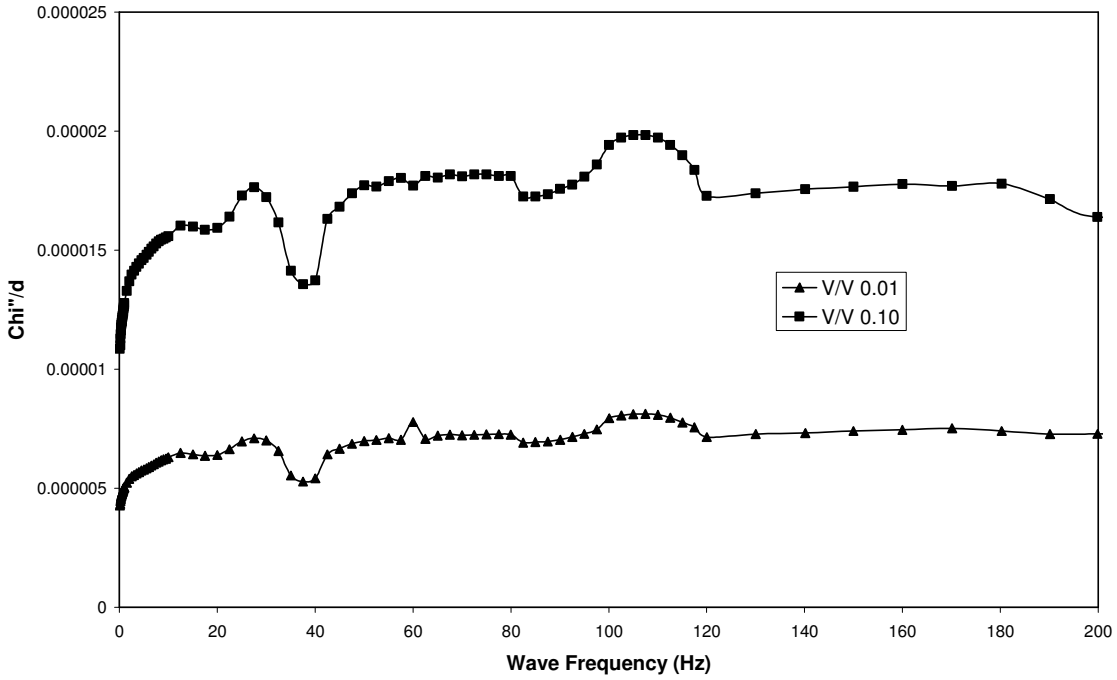


**Figure 30 Out-of-phase component of the AC susceptibility for PEO nanofibers containing v/v 0.01 and v/v 0.10 magnetite nanoparticles**

The two fiber samples tested had basically identical spectra pattern. Distinct peaks were seen in both fibers at 30 Hz, 40 Hz, and 110 Hz. These distinct peaks are characteristic properties of the magnetic domains inside of the fibers.

## 4.4 ALTERNATING MAGNETIC FIELD

Experiments were performed to combine an alternating magnetic field with the parallel plate electrospinning set-up. Initially the solenoid was placed on the top plate of the electrospinning apparatus as shown in Figure 31. Prior to beginning electrospinning, an amplitude value of 3-4 amps was supplied to the solenoid to create the alternating magnetic field with a frequency of 1 kHz.

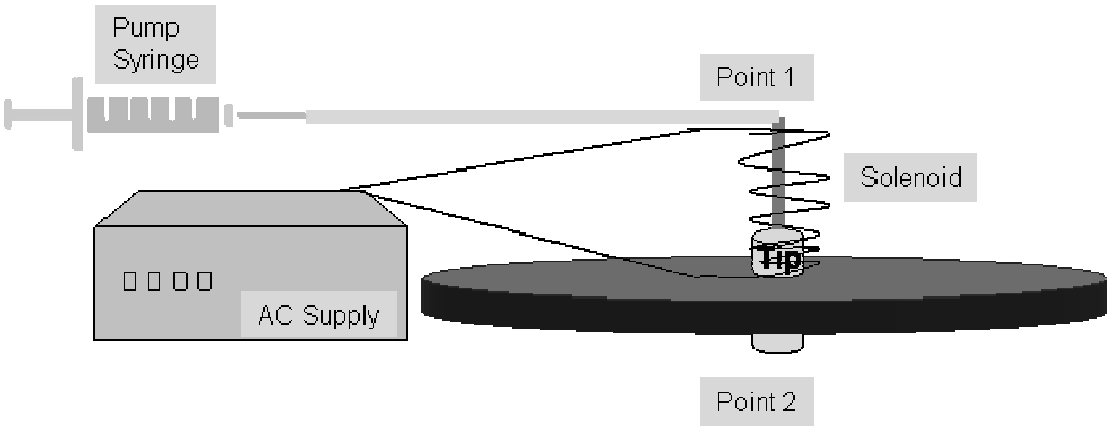


**Figure 31 Electrospinning set-up #1 with AC magnetic field capabilities**

Using a gauss meter, a magnetic field force of ~21 Gauss was measured at Point 1 on the solenoid, but a force of only 0.3 Gauss was detected at the tip exit located on the underside of the top plate. Aluminum is nonmagnetic, and its relative magnetic permeability is approximately 1, therefore it is as permeable as air. The aluminum permeability is such that it should not prevent the field from permeating to Point 2. It was concluded that the distance from the solenoid to the tip exit was beyond the range of the magnetic field.

Next a 30 gauge copper wire was used that would allow the solenoid to go through the top plate aperture, as shown in Figure 32. The solenoid extended to the exit of the tip.

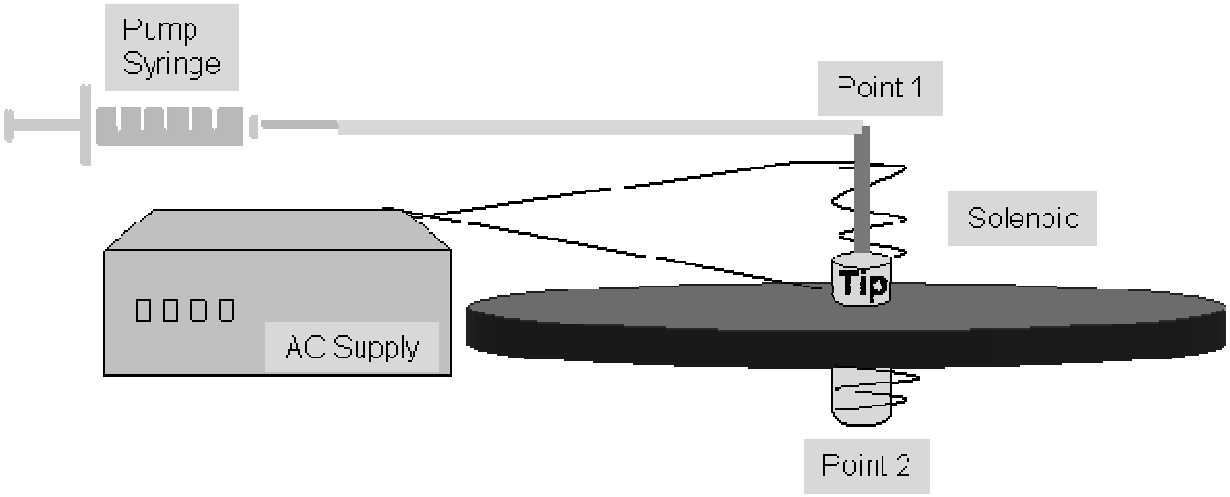


**Figure 32 Electrospinning set-up #2 with AC magnetic field capabilities**

This set-up allowed the field force to be perpetuated onto both sides of the solenoid equally with a value of 21 Gauss. The amplitude of the current caused the wire to begin to burn and disintegrate. It was discovered that the higher gauge wire could not support the desired AC current amplitude.

Finally to supply the alternating magnetic field, the solenoid was placed between the two electrospinning plates.

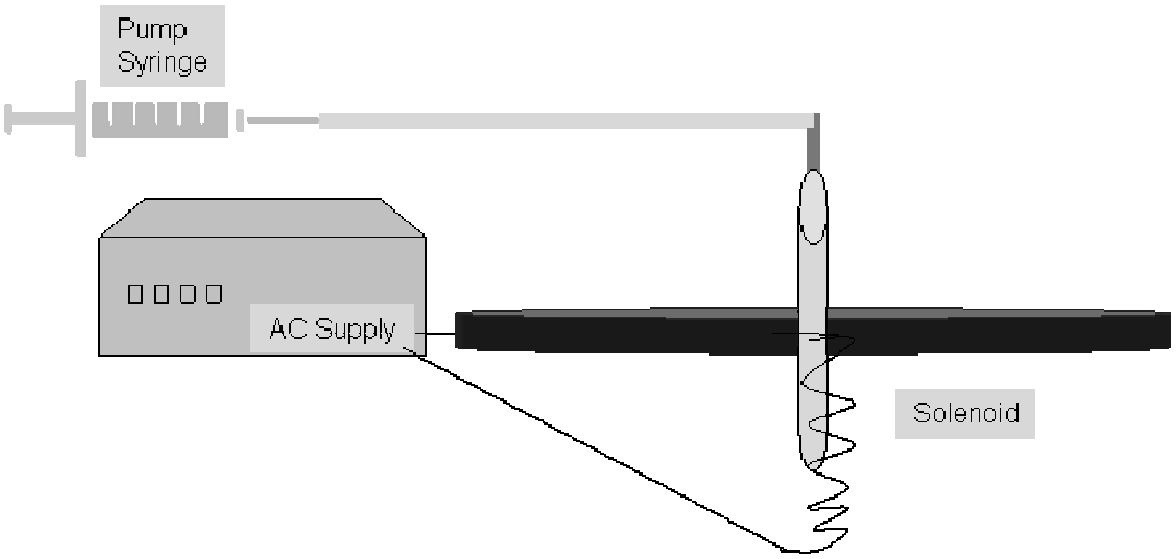


**Figure 33 Electrospinning set-up #3 with AC magnetic field capabilities**

The set-up shown in Figure 33 allowed for the use of the original lower gauge magnet wire capable of withstanding the desired current amplitude. The combination of the magnetic field and the electrospinning voltage created arcing. Arcing occurs when an electrical current discharge moves from one electrode to another. This prevented the experiment form continuing without damaging the equipment. By switching the positive and negative electrodes on the plates, arcing was avoided; however this led to electrospinning to occur from the bottom up as demonstrated in Figure 33. The unevaporatated solution on the bottom plate collected enough charge to

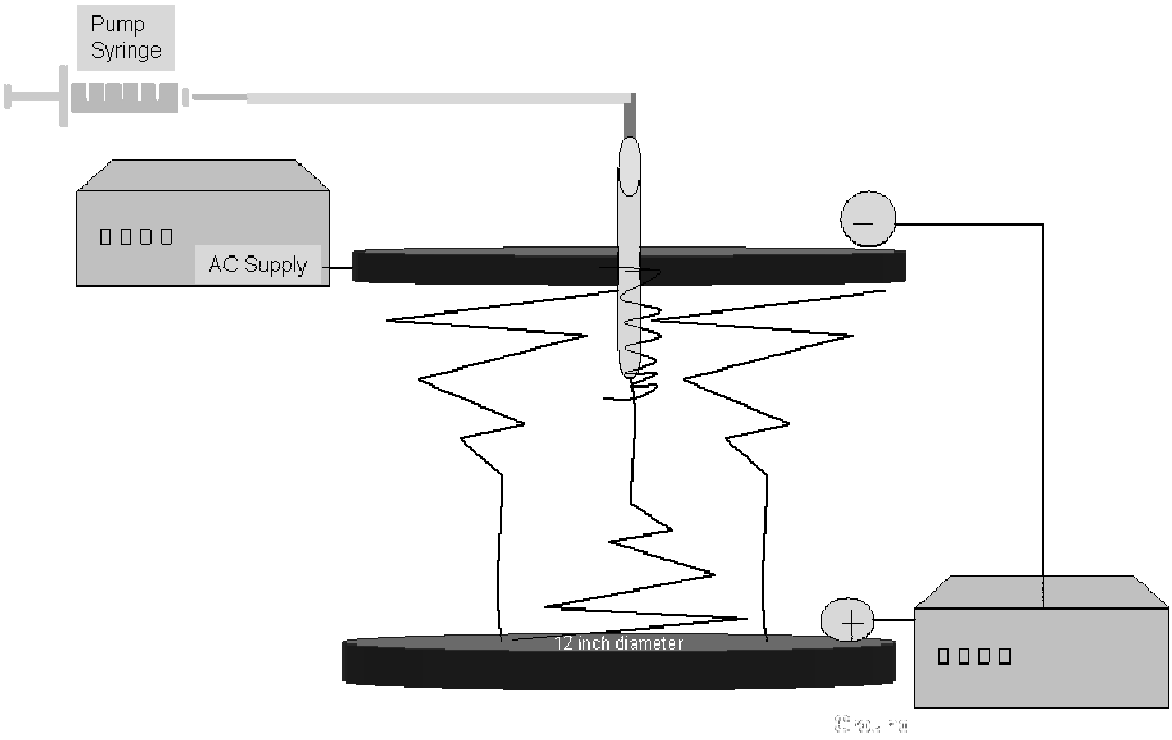


**Figure 34 Backward Electrospinning Schematic**

create an attraction to the top plate. The fibers flowing from bottom up, interfered with flow from the tip; thereby making the electrospinning process discontinuous.

# 5 CONCLUSIONS

Nanocomposite polyethylene oxide (PEO) fibers containing individual magnetic domains were spun using parallel plate electrospinning. The fibers were spun from solutions dosed with nanoparticles of magnetite ($Fe_3O_4$) at various loading fractions in 2 wt% PEO in water. A high (v/v 0.10) and a low (v/v 0.01) magnetite dosed solution were used to determine how the processing parameters and fiber properties changed as a function of nanoparticle concentration.

The inclusion of the magnetic nanoparticles produced solutions with higher conductivity, lower surface tension, and higher viscosity. Phase diagrams were constructed to show the three regions: dripping, stable, and whipping. Higher viscosity solutions were spun without significantly higher electric field requirements due to the reduction in surface tension and higher conductivity.

Electrospinning was used to produce fibers with diameters as low as 45 nanometers. Transmission electron microscopy showed that the average fiber diameter increased with increasing magnetite concentration. Energy dispersive spectroscopy showed an increase in iron characteristic x-rays for the higher loading fiber samples. The saturation and remnant magnetization was higher for v/v 0.10 fibers due to the contribution of the domain alignment. Unique AC susceptibility signatures were identified using SQUID analysis methods.

# 6 SUGGESTIONS FOR FURTHER RESEARCH

Many possibilities exist for future work in the area of electrospinning nanofibers. Currently energy requirements for the electrospinning process limit its feasibility as a full scale production process. This work identified new avenues that future researchers can use to lower the energy requirements.

The first suggestion involves analyzing the effect of the capillary tip. Two tips were used during this research: a aluminum tip (i.d.0.75 mm) and a glass tip (i.d.1.5 mm). The difference between the two reside in the materials of construction and the tip size. Phase diagrams were constructed using the glass capillary tip and the applied voltage to achieve stable and whipping flow was dramatically reduced compared to the energy requirements of the metal tip.

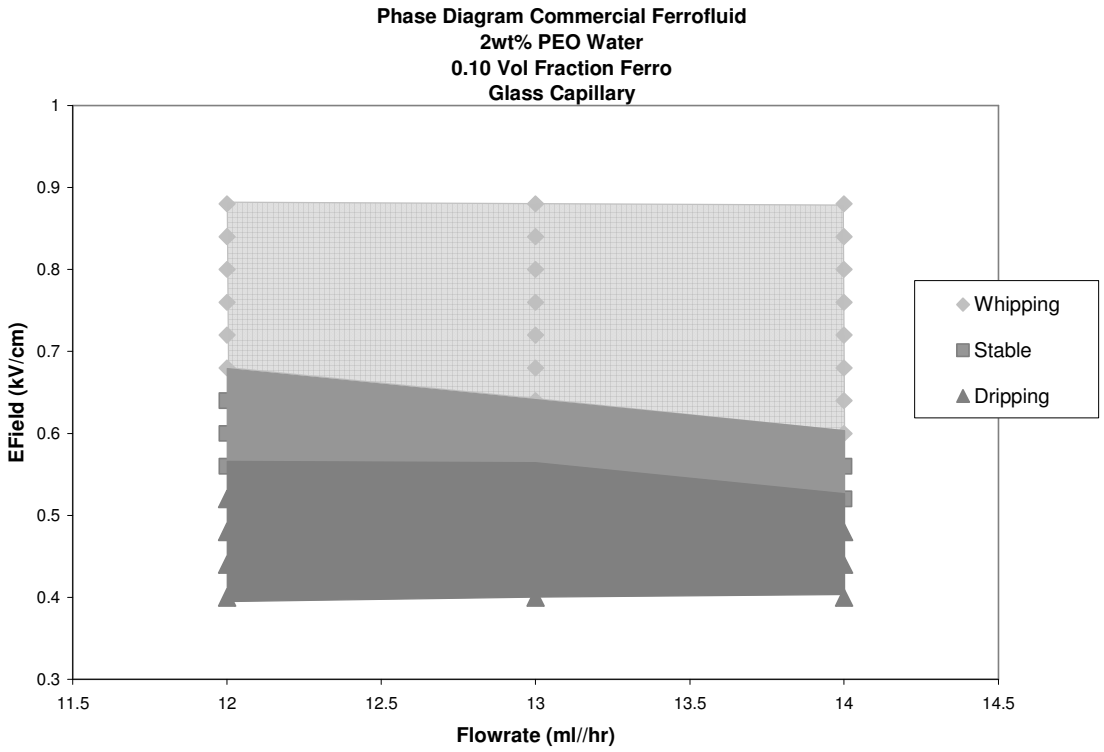


**Figure 35 Magnetite/ PEO (containing v/v 0.10 magnetite) electrospinning phase diagram depicting the flow rate and electric field for dripping, stable, and whipping flow using glass tip**

For identical processing parameters, 19 kV and 45 kV were required for whipping with the glass and aluminum capillaries respectively. This reduction is attributed to the ease at which the charge was able to contact the solution with the glass tip. The walls of the glass tip were 0.3 mm compared to ~ 3mm for the aluminum tip. Future investigation is suggested to explore the impact of the effect of tip size and material of construction.

The negative viscosity effect theoretically supplies a way to alter solution viscosity, the most important factor in determining final fiber diameter. Modifications to the electrospinning set-up can provide alternatives for incorporating the AC magnetic field:

(a) A top plate with larger aperture that can accommodate a solenoid of magnetic wire insulated by a dielectric material to prevent arcing

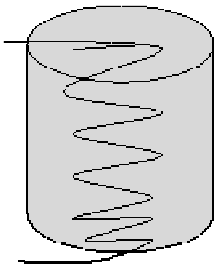

**Figure 36 Recommended solenoid enclosed in dielectric material for electrospinning with AC magnetic field**

(b) Electrically connect the solenoid to the electrospinning plates to prevent arcing

Either suggestion (a) or (b) could allow for the incorporation of the alternating magnetic field into the electrospinning set-up.

Finally, particle agglomeration occurred in samples with lower concentration of magnetite. Functionalizing the particles with a layer of PEO could improve the dispersion of the particles within the polymer solutions. The University of Puerto Rico at Mayaguez synthesized thiolated nanoparticles with PEO. Below is a micrograph of v/v 0.01 loading of the modified particles.

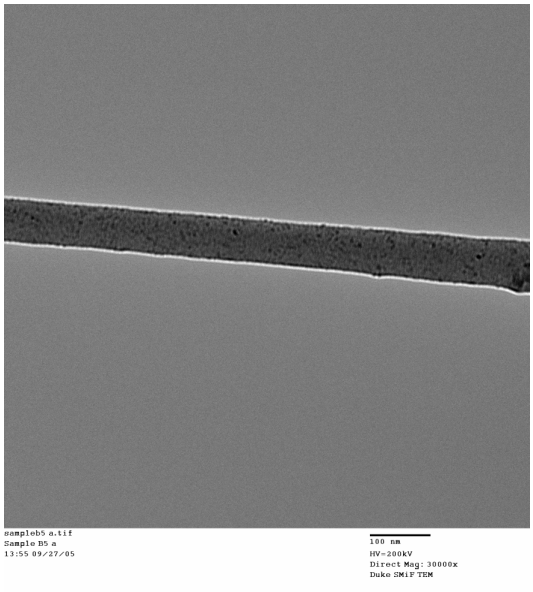


**Figure 37 TEM micrograph of PEO nanofiber containing 0.01 v/v functionalized magnetite nanoparticles**

This functionalization greatly improved the particle dispersion within the fiber matrix and warrants further investigation.

## 7 REFERENCES


1. Lubbe, A.S., C. Alexiou, and C. Bergemann, *Clinical applications of magnetic drug targeting.* Journal of Surgical Research, 2001. **95**(2): p. 200-206.

2. Wilson, J.L., et al., *Synthesis and magnetic properties of polymer nanocomposites with embedded iron nanoparticles.* Journal of Applied Physics, 2004. **95**(3): p. 1439-1443.

3. Verma, S. and P.A. Joy, *Magnetic properties of superparamagnetic lithium ferrite nanoparticles.* Journal of Applied Physics, 2005. **98**(12).

4. Marchessault, R.H., P. Rioux, and L. Raymond, *Magnetic Cellulose Fibers and Paper - Preparation, Processing and Properties.* Polymer, 1992. **33**(19): p. 4024-4028.

5. Huang, Z.M., et al., *A review on polymer nanofibers by electrospinning and their applications in nanocomposites.* Composites Science and Technology, 2003. **63**(15): p. 2223-2253.

6. Spivak, A.F., Y.A. Dzenis, and D.H. Reneker, *A model of steady state jet in the electrospinning process.* Mechanics Research Communications, 2000. **27**(1): p. 37-42.

7. Li, D. and Y.N. Xia, *Electrospinning of nanofibers: Reinventing the wheel?* Advanced Materials, 2004. **16**(14): p. 1151-1170.

8. Theron, S.A., E. Zussman, and A.L. Yarin, *Experimental investigation of the governing parameters in the electrospinning of polymer solutions.* Polymer, 2004. **45**(6): p. 2017-2030.

9. Hohman, M.M., et al., *Electrospinning and electrically forced jets. II. Applications.* Physics of Fluids, 2001. **13**(8): p. 2221-2236.

10. Hohman, M.M., et al., *Electrospinning and electrically forced jets. I. Stability theory.* Physics of Fluids, 2001. **13**(8): p. 2201-2220.

11. Li, D., T. Herricks, and Y.N. Xia, *Magnetic nanofibers of nickel ferrite prepared by electrospinning.* Applied Physics Letters, 2003. **83**(22): p. 4586-4588.

12. Demir, M.M., et al., *Electrospinning of polyurethane fibers.* Polymer, 2002. **43**(11): p. 3303-3309.

13. Duan, B., et al., *Electrospinning of chitosan solutions in acetic acid with poly(ethylene oxide).* Journal of Biomaterials Science-Polymer Edition, 2004. **15**(6): p. 797-811.

14. Mit-uppatham, C., M. Nithitanakul, and P. Supaphol, *Ultratine electrospun polyamide-6 fibers: Effect of solution conditions on morphology and average fiber diameter.* Macromolecular Chemistry and Physics, 2004. **205**(17): p. 2327-2338.

15. Reneker, D.H. and I. Chun, *Nanometre diameter fibres of polymer, produced by electrospinning.* Nanotechnology, 1996. **7**(3): p. 216-223.

16. Zhao, Y.Y., et al., *Study on correlation of morphology of electrospun products of polyacrylamide with ultrahigh molecular weight.* Journal of Polymer Science Part B-Polymer Physics, 2005. **43**(16): p. 2190-2195.

17. Zhao, Z.Z., et al., *Preparation and properties of electrospun poly(vinylidene fluoride) membranes.* Journal of Applied Polymer Science, 2005. **97**(2): p. 466-474.

18. Ristolainen, N., et al., *Poly(vinyl alcohol) and polyamide-66 nanocomposites prepared by electrospinning.* Macromolecular Materials and Engineering, 2006. **291**(2): p. 114-122.

19. Gupta, P., et al., *Electrospinning of linear homopolymers of poly(methyl methacrylate): exploring relationships between fiber formation, viscosity, molecular weight and concentration in a good solvent.* Polymer, 2005. **46**(13): p. 4799-4810.

20. Pornsopone, V., et al., *Electrospinning of methacrylate-based copolymers: Effects of solution concentration and applied electrical potential on morphological appearance of as-spun fibers.* Polymer Engineering and Science, 2005. **45**(8): p. 1073-1080.

21. Deitzel, J.M., et al., *The effect of processing variables on the morphology of electrospun nanofibers and textiles.* Polymer, 2001. **42**(1): p. 261-272.

22. Kalayci, V.E., et al., *Charge consequences in electrospun polyacrylonitrile (PAN) nanofibers.* Polymer, 2005. **46**(18): p. 7191-7200.

23. Doshi, J. and D.H. Reneker, *Electrospinning Process and Applications of Electrospun Fibers.* Journal of Electrostatics, 1995. **35**(2-3): p. 151-160.

24. Tan, S.H., et al., *Systematic parameter study for ultra-fine fiber fabrication via electrospinning process.* Polymer, 2005. **46**(16): p. 6128-6134.

25. Lee, C.K., S.I. Kim, and S.J. Kim, *The influence of added ionic salt on nanofiber uniformity for electrospinning of electrolyte polymer.* Synthetic Metals, 2005. **154**(1-3): p. 209-212.

26. Shin, Y.M., et al., *Experimental characterization of electrospinning: the electrically forced jet and instabilities.* Polymer, 2001. **42**(25): p. 9955-9967.

27. Yang, Q.B., et al., *Influence of solvents on the formation of ultrathin uniform poly(vinyl pyrrolidone) nanofibers with electrospinning.* Journal of Polymer Science Part B-Polymer Physics, 2004. **42**(20): p. 3721-3726.

28. Jarusuwannapoom, T., et al., *Effect of solvents on electro-spinnability of polystyrene solutions and morphological appearance of resulting electrospun polystyrene fibers.* European Polymer Journal, 2005. **41**(3): p. 409-421.

29. Fridrikh, S.V., et al., *Controlling the fiber diameter during electrospinning.* Physical Review Letters, 2003. **90**(14).

30. Shin, Y.M., et al., *Electrospinning: A whipping fluid jet generates submicron polymer fibers.* Applied Physics Letters, 2001. **78**(8): p. 1149-1151.

31. Reneker, D.H., et al., *Bending instability of electrically charged liquid jets of polymer solutions in electrospinning.* Journal of Applied Physics, 2000. **87**(9): p. 4531-4547.

32. Serway, R.A., *Physics for Scientists and Engineers*. 4th ed. 1996, Chicago: Saunders College Publishing.

33. Jiles, D.C., *Recent advances and future directions in magnetic materials.* Acta Materialia, 2003. **51**(19): p. 5907-5939.

34. Rosensweig, R.E., *Ferrohydrodynamics*. 1985: Cambridge University Press.

35. Poddar, P., et al., *Magnetic properties of conducting polymer doped with manganese-zinc ferrite nanoparticles.* Nanotechnology, 2004. **15**(10): p. S570-S574.

36. Chikazumi, S., et al., *Physics of Magnetic Fluids.* Journal of Magnetism and Magnetic Materials, 1987. **65**(2-3): p. 245-251.

37. Zhang, Y.D., et al., *Effect of spin disorder on magnetic properties of nanostructured Ni-ferrite.* Journal of Applied Physics, 2004. **95**(11): p. 7130-7132.

38. Odenbach, S., *Recent progress in magnetic fluid research.* Journal of Physics-Condensed Matter, 2004. **16**(32): p. R1135-R1150.

39. Zahn, M., *Magnetic fluid and nanoparticle applications to nanotechnology.* Journal of Nanoparticle Research, 2001. **3**(1): p. 73-78.

40. Rosensweig, R.E., *"Negative viscosity" in a magnetic fluid.* Science, 1996. **271**(5249): p. 614-615.

41. Zeuner, A., R. Richter, and I. Rehberg, *Experiments on negative and positive magnetoviscosity in an alternating magnetic field.* Physical Review E: Statistical Physics, Plasmas, Fluids, and Related Interdisciplinary Topics, 1998. **58**(5-B): p. 6287-6293.

42. Rinaldi, C., et al., *Torque measurements on ferrofluid cylinders in rotating magnetic fields.* Journal of Magnetism and Magnetic Materials, 2005. **289**: p. 307-310.

43. Bacri, J.C., et al., *Negative-Viscosity Effect in a Magnetic Fluid.* Physical Review Letters, 1995. **75**(11): p. 2128-2131.

44. Goldstein, J.I., *Scanning Electron Microscopy and X-ray Microanalysis*. 2003: Kluwer Academic/ Plenum Publishing.

45. http://www.unl.edu/CMRAcfem/temoptic.htm.

46. Kroell, M., et al., *Magnetic and rheological characterization of novel ferrofluids.* Journal of Magnetism and Magnetic Materials, 2005. **289**: p. 21-24.

47. Lu, X.F., et al., *Preparation and characterization of Ag2S nanoparticles embedded in polymer fibre matrices by electrospinning.* Nanotechnology, 2005. **16**(10): p. 2233-2237.

48. Carpenter, E.E., *Iron nanoparticles as potential magnetic carriers.* Journal of Magnetism and Magnetic Materials, 2001. **225**(1-2): p. 17-20.

49. Norton, D.P., et al., *Ferromagnetism in cobalt-implanted ZnO.* Applied Physics Letters, 2003. **83**(26): p. 5488-5490.

50. Mikhaylova, M., et al., *Superparamagnetism of magnetite nanoparticles: Dependence on surface modification.* Langmuir, 2004. **20**(6): p. 2472-2477.

51. Sun, X.C., *Microstructure characterization and magnetic properties of nanomaterials.* Molecular Physics, 2002. **100**(19): p. 3059-3063.

**APPENDICES**

## APPENDIX A: CALCULATIONS

### Volume Fraction Calculations

**To determine the volume fraction PEO in 2 wt% PEO/water solution**

$$\frac{0.02 \times 0.99 \ \frac{g}{ml}}{1.14 \ \frac{g}{ml}} = 0.017 \ \frac{v}{v}$$

**To determine the volume PEO in 20 ml sample**

$$0.017 \frac{ml \ PEO}{ml \ solution} \times 20 \ ml \ \ solution = 0.34 \ ml \ \ PEO$$

**To determine the volume of $Fe_3O_4$ needed for v/v 0.01**

$$\frac{0.01 \ ml \ \ Fe_3O_4}{ml \ \ PEO} \times 0.34 \ ml \ \ PEO = 0.0034 \ \ ml \ \ Fe_3O_4$$

**To determine the volume of ferrofluid needed for v/v 0.01**

$$\frac{0.0034 \ \ ml \ \ Fe_3O_4}{} \times \frac{ml \ \ Ferrofluid}{0.036 \ \ ml \ \ Fe_3O_4} = 0.10 \ ml \ Ferrofluid$$

**Weight Percent Calculations**

**To determine the weight percent $Fe_3O_4$ in final fiber**

$$\frac{0.01 ml\ Fe_3O_4}{ml\ PEO} \times \frac{ml}{1.14 g} \times \frac{5.2\ g}{ml\ Fe_3O_4} = 4.5\ wt\%\ Fe_3O_4$$

$$\frac{0.10 ml\ Fe_3O_4}{ml\ PEO} \times \frac{ml}{1.14 g} \times \frac{5.2\ g}{ml\ Fe_3O_4} = 45.6\ wt\%\ Fe_3O_4$$

**To determine the weight percent $Fe_3O_4$ in electrospinning solutions**

**For fiber containing v/v 0.01 magnetite/ PEO:**

$$\frac{20\ ml\ PEO/water}{} \times \frac{0.99\ g}{ml} = 19.8\ g\ PEO/water$$

$$\frac{0.036 ml\ Fe_3O_4}{ml\ Ferrofluid} \times \frac{0.10\ ml\ Ferrofluid}{} \times \frac{5.2\ g\ Fe_3O_4}{ml\ Fe_3O_4} = 0.0187\ g\ Fe_3O_4$$

$$\frac{0.934 ml\ H_2O}{ml\ Ferrofluid} \times \frac{0.10\ ml\ Ferrofluid}{} \times \frac{1.00\ g\ H_2O}{ml\ H_2O} = 0.093\ g\ H_2O$$

$$\frac{0.0187\ g\ Fe_3O_4}{19.8\ g\ PEO/water + 0.0187\ g\ Fe_3O_4 + 0.093\ g\ H_2O} = 0.094\ wt\%\ Fe_3O_4$$

**For fiber containing v/v 0.01 magnetite/ PEO:**

$$\frac{20\ ml\ \ PEO/water}{} \times \frac{0.99\ \ g}{ml} = 19.8\ \ g\ \ PEO/water$$

$$\frac{0.036\,ml\ \ Fe_3O_4}{ml\ Ferrofluid} \times \frac{1.10\ ml\ \ Ferrofluid}{} \times \frac{5.2\ \ g\ \ Fe_3O_4}{ml\ Fe_3O_4} = 0.296\,g\ Fe_3O_4$$

$$\frac{0.934\,ml\ \ H_2O}{ml\ Ferrofluid} \times \frac{1.10\ ml\ \ Ferrofluid}{} \times \frac{1.00\,g\ H_2O}{ml\ H_2O} = 1.03\,g\ H_2O$$

$$\frac{0.296\,g\ Fe_3O_4}{19.8\,g\ PEO/water + 0.296\,g\ Fe_3O_4 + 1.03\,g\ H_2O} = 1.40\,wt\%\ \ Fe_3O_4$$

**Constants Used in Calculations:**

- Density of 2wt% PEO/ water: 0.99 g/ml
- Density of PEO : 1.14 g/ml
- Volume Fraction $Fe_3O_4$ in MSG W11 ferrofluid : 0.036 ml/ml
- Density of $Fe_3O_4$ : 5.2 g/ml

## APPENDIX B: VISCOSITY DATA

Viscosity Measurement 2wt% PEO/ Water

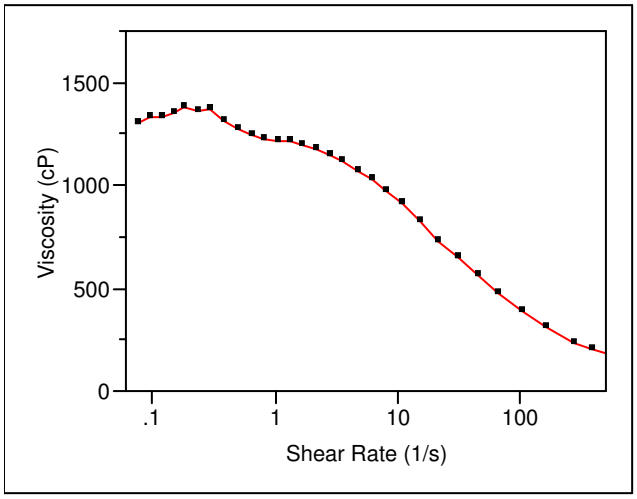


Viscosity Measurement Ferrofluid

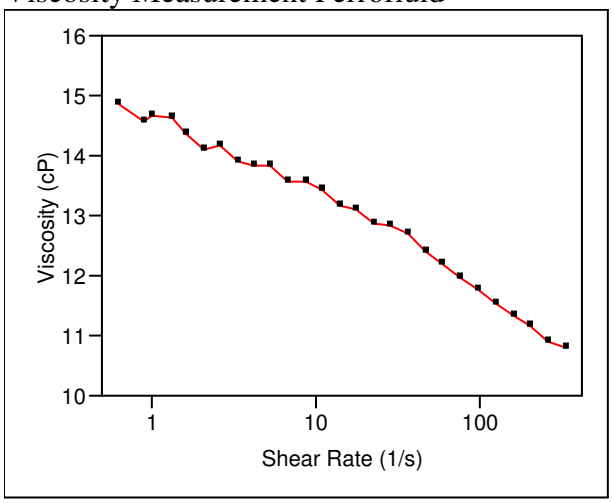

Viscosity Measurement Magnetite/PEO v/v 0.10

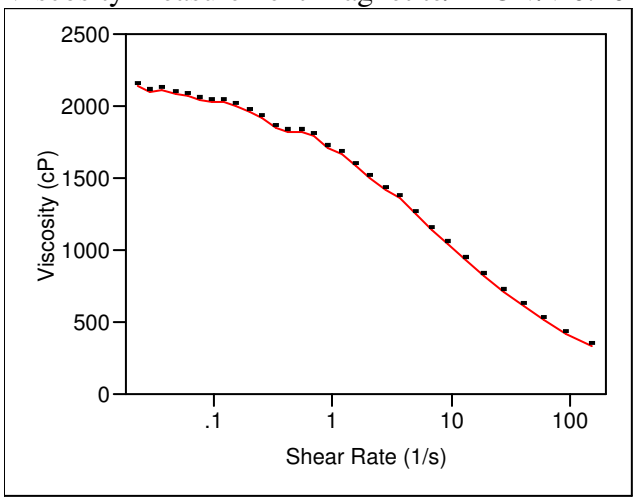


Viscosity Measurement Magnetite/PEO v/v 0.01